

This manuscript is a pre-print and has been submitted for publication in the Basin Research journal. Please note this manuscript has not been peer-reviewed, subsequent versions of the manuscript may vary. If accepted, the final version of this manuscript will be available via the 'Peer-reviewed Publication DOI' link to the right of this webpage. Please do not hesitate to contact the authors with any questions or feedback.

Multi-layered salt-prone stratigraphy and its influence on rift-basin development; The Slyne and Erris basins, offshore NW Ireland

Conor M. O'Sullivan^{1,2}, Conrad J. Childs^{1,2}, Muhammad M. Saqab^{1,2*}, John J. Walsh^{1,2}, Patrick M. Shannon^{1,3}

¹ Irish Centre for Research in Applied Geoscience (iCRAG), University College Dublin, Belfield, Dublin 4, Ireland

² Fault Analysis Group, School of Earth Sciences, University College Dublin, Belfield, Dublin 4, Ireland

³ School of Earth Sciences, University College Dublin, Belfield, Dublin 4, Ireland

*Present Address: Norwegian Geotechnical Institute, 40 St. Georges Terrace, Perth, WA 6000, Australia

Corresponding author email: conor.osullivan@icrag-centre.org

Abstract:

While salt-influenced rift basins have been identified across the European Atlantic margin, the Irish Atlantic margin remains the exception despite salt being proven in several boreholes. Using an extensive seismic database coupled with data from exploration wells and shallow boreholes, this study maps the distribution and composition of salt layers and investigates their role in the structural evolution of the Slyne and Erris basins offshore west of Ireland. Two salt-prone intervals have been proven: The Upper Permian Zechstein Group and the Upper Triassic Uilleann Halite Member. The Zechstein Group is present throughout the Slyne and Erris basins, while the Uilleann Halite Member is only developed in the Northern Slyne and Southern Erris sub-basins. Where salt-prone, both layers mechanically detach pre-, post-, and intra-salt stratigraphy. Both layers underwent halokinesis during basin development, creating a variety of salt-related structures; The Zechstein Group forms salt pillows and salt rollers, causing folding and rafting in the overlying Mesozoic section, driven by active faulting within the pre-salt basement. The Uilleann Halite Member caused thin-skinned crestal collapse of the overlying Jurassic section above anticlines cored by Zechstein salt. Where both Triassic and Permian salt are present, unique structural geometries are formed when two stratigraphically discrete but kinematically linked halokinetic structures develop. The most common structural configuration consists of a Zechstein salt pillow and an Uilleann Halite salt wall separated by Lower Triassic sandstones. The fold-axis of the salt pillow trends parallel to the strike of the salt wall. The results of this study provide a framework for the evolution of halokinetic structures in other basins on the Irish Atlantic margin, greater insight into the Permian and Triassic paleogeography of the region, as well as having more general implications for the evolution of salt-related structures in rift basins with multiple stratigraphically discrete salt layers.

35 Acknowledgements

36 This research is funded in part by a research grant from Science Foundation Ireland (SFI)
37 under Grant Number 13/RC/2092 and is co-funded under the European Regional
38 Development Fund, and by the Petroleum Infrastructure Programme (PIP) and its member
39 companies. Efstratios Delogkos is thanked for thoughtful discussions regarding the links
40 between the Slyne and Erris basins and the Bróna and Pádraig basins. Neil Jones and Kristian
41 Lomas are thanked for engaging discussions on the structural evolution of the Slyne and
42 Goban Spur basins respectively. The authors would like to thank the Petroleum Affairs Division
43 (PAD) of the Department of Communications, Climate Action and Environment (DCCAE),
44 Ireland, for providing access to released well, seismic, and potential field datasets. Europa Oil
45 & Gas are thanked for providing access to the Inishkea 2018 reprocessed seismic volume and
46 allowing a section from the volume to be shown. Shell Exploration & Production Ireland Ltd.
47 are thanked for providing access to reprocessed volumes of the 1997 Corrib seismic. The
48 authors would also like to thank Schlumberger for providing academic licenses of Petrel to
49 University College Dublin.

50 Data Availability Statement

51 The data that support the findings of this study were provided by the Petroleum Affairs Division
52 (PAD) and are available for download from [https://www.dccae.gov.ie/en-ie/natural-
53 resources/topics/Oil-Gas-Exploration-Production/data/Pages/Data.aspx](https://www.dccae.gov.ie/en-ie/natural-resources/topics/Oil-Gas-Exploration-Production/data/Pages/Data.aspx). Restrictions may
54 apply to the availability of these data, which were used under licence for this study.

55 1. Introduction:

56 Salt plays an important role in the development of sedimentary basins, acting as a layer of
57 mechanical detachment between pre- and post-salt stratigraphy. This leads to significant
58 differences in the structural styles and evolution of salt-influenced basins relative to those
59 unaffected by salt. Thick layers of salt have been encountered in several basins across the
60 European Atlantic margin, including offshore Iberia (Alves et al., 2006; Pena dos Reis et al.,
61 2017; Ramos et al., 2017; Zamora et al., 2017), offshore France (Chapman, 1989; Ferrer et
62 al., 2012), on the United Kingdom Continental Shelf (UKCS) (Stewart et al., 1996; Jackson &
63 Stewart, 2017) and offshore Norway (Jackson et al., 2019; Rojo et al., 2019). Salt is also
64 present in basins on the conjugate margin of Atlantic Canada (Jansa et al., 1980; Deptuck &
65 Kendell, 2017). In these areas, the main layers of salt range in age from Early Permian to
66 Early Jurassic, and have had a profound impact on basin development, commonly having
67 undergone significant halokinesis to form distinctive salt-related structures such salt diapirs
68 and allochthonous salt sheets and canopies.

69 The Irish Atlantic margin has seen comparatively little research investigating the presence and
70 impact of salt, owing to the limited well penetrations and lack of characteristic salt-related
71 structures on seismic data. Nevertheless, Upper Triassic salt is proven in the Celtic Sea basins
72 (Robinson et al., 1981; Van Hoorn, 1987; Shannon, 1991), the Central Irish Sea and St.
73 Georges Channel basins (Naylor & Shannon, 1982) and the Kish Bank Basin (Naylor et al.,
74 1993; Dunford et al., 2001). In the Porcupine Basin, Croker & Shannon (1987) reported the
75 presence of salt in two wells in the north of the basin, while the 35/19-1 well encountered 24m
76 of what is believed to be Upper Triassic allochthonous salt that is intruded into Upper Jurassic
77 sediments (Britoil, 1986). Salt has also been identified onshore Ireland, within the Ulster-Larne
78 Basin of Northern Ireland (Illing & Griffith, 1986; McCann, 1988; Quinn et al., 2010) and in a
79 small outlier at Kingscourt, Co. Cavan (Gardiner & Visscher, 1971; Gardiner & McArdle, 1992).
80 Previous work has identified the presence of salt in the Slyne and Erris basins (Tate & Dobson,
81 1989; Chapman et al., 1999; Dancer et al., 1999; Dancer et al., 2005) but limited and poor-
82 quality seismic data, coupled with few well penetrations, made it difficult to analyse the impact
83 of these salt-prone layers on basin development. Since then, significantly more seismic data
84 has been acquired and additional exploration wells have been drilled, allowing the nature of
85 salt and the role it plays in the evolution of the Slyne and Erris basins to be investigated in
86 greater detail (Fig. 1).

87 This study utilizes an extensive database of 2D and 3D multichannel seismic reflection data,
88 coupled with wireline, cuttings and core data from exploration wells and shallow boreholes to
89 understand the distribution and composition of salt in the Slyne and Erris basins, and the

90 impact of salt on the structural evolution of these basins. Both Upper Permian and Upper
91 Triassic salt layers have now been identified over significant parts of the study area, the
92 Zechstein Group and Uilleann Halite Member respectively. The Uilleann Halite Member is
93 termed the Mercia Halite Member in previous literature (e.g. Corcoran & Mecklenburgh, 2005;
94 Dancer et al., 2005). This unique condition results in stacked salt-related structures with
95 evidence for interaction between halokinetic features developed at different structural levels.
96 In our study the distribution of salt on the Irish Atlantic margin is placed in regional context to
97 provide insights into Late Permian and Late Triassic paleogeography, and the influence of salt
98 on the petroleum systems of the Slyne and Erris basins.

99 2. Geological Setting:

100 The Slyne and Erris basins are contiguous rift basins located on the Irish Mainland Shelf off
101 the north-western coast of Ireland in water depths of 150m to 3000m. They are narrow,
102 elongate and broadly NE-SW oriented basins, which belong to a framework of rift basins
103 extending westward from the coast of Ireland across the Irish Atlantic margin to the Atlantic
104 Abyssal Plain, and form part of chain of rift basins stretching along the European Atlantic
105 margin from the Barents Sea offshore northern Norway to offshore Portugal. These rift basins
106 formed during episodic extensional periods beginning with Variscan orogenic collapse and
107 culminating with the onset of oceanic crust formation in the North Atlantic Ocean during the
108 Eocene (Doré et al., 1999, Stoker et al., 2017; Schiffer et al., 2019).

109 2.1. Tectonostratigraphic evolution of the Slyne and Erris 110 basins:

111 The Slyne and Erris basins began to form during the Permian breakup of Pangea. Extension
112 created a series of narrow, NE-SW and NNE-SSW oriented half-grabens, with the polarity of
113 individual half-grabens varying from westward-dipping to eastward-dipping along strike (Fig.
114 1; Chapman et al., 1999; Dancer et al., 1999). The arid Permian climate led to the formation
115 of thick evaporite deposits in the hanging-walls of active faults, while carbonates and clastics
116 were deposited on the basin margins (Stoker et al., 2017). Extension ceased by the Early
117 Triassic, with thick fluvial and aeolian sandstones being deposited regionally (Štolfová &
118 Shannon, 2009). This was followed by the widespread deposition of playa-lake mudstones
119 and siltstones and locally thick halite deposits during the Late Triassic (Figs 1 & 2).

120 The end of the Triassic was marked by a regional marine transgression and the deposition of
121 shallow marine limestones, sandstones and mudstones during the Rhaetian to the Sinemurian
122 (Trueblood & Morton, 1991; Raine et al., 2020). The area experienced mild extension during
123 this time, with subtle syn-extensional thickening of the Lower Jurassic section occurring in the
124 hanging-walls of active basin-bounding faults (Dancer et al., 1999). Intrabasinal NE-SW and
125 NNE-SSW oriented listric faults formed throughout the basin above small salt rollers and salt
126 pillows. A minor break during the early Pliensbachian created a subtle unconformity, above
127 which Late Pliensbachian to Bajocian marine sandstones, limestones and mudstones were
128 deposited.

129 A major unconformity separates the Lower and Middle Jurassic marine sediments from the
130 overlying Upper Jurassic fluviio-estuarine sediments, with the unconformity locally incising
131 deeply enough to locally place the Oxfordian onto the Pliensbachian and Sinemurian on the

132 margins of the basin. The main phase of rifting occurred during this time, with movement on
133 basin-bounding faults creating accommodation space for the deposition of several kilometres
134 of Upper Jurassic sediments (IS16/04 Technical Report, 2019). The Upper Jurassic sediments
135 consist of Oxfordian-aged terrestrial, fluvial and estuarine sandstones and mudstones with
136 associated coal horizons, which grade upwards into marine mudstones, limestones and
137 sandstones, indicating a regional marine transgression occurred during the Kimmeridgian and
138 Tithonian (Fig. 2).

139 Rifting in the Slyne and Erris basins ceased at the end of the Jurassic, with the area
140 experiencing kilometre-scale uplift and erosion during the Early Cretaceous. As rifting
141 occurred in the Rockall Basin to the west, the Erris Basin in particular was subject to severe
142 rift-shoulder uplift, undergoing greater uplift along the western margin of the basin while thick
143 Cretaceous sediments were deposited along the basin's eastern margin (Chapman et al.,
144 1999; Walsh et al., 1999). Areas that were separated from the Rockall Basin by intervening
145 basement highs, such as the Erris Ridge, did not experience the same extent of rift-shoulder
146 uplift. The Slyne Basin remained a relative high throughout the Cretaceous, shielded from rift-
147 related subsidence in the Rockall Basin by the Porcupine High, with only a thin veneer of
148 Lower and Upper Cretaceous sediments deposited throughout the basin.

149 As rifting in the Rockall Basin ceased towards the end of the Cretaceous, the basin underwent
150 thermal subsidence, with the western margins of the northern Slyne and the Erris basins that
151 had been subject to rift-shoulder uplift now experiencing large-scale subsidence. Post-rift
152 tectonic activity continued throughout the Paleocene, Eocene and Early Miocene, expressed
153 as subtle normal and reverse movement on faults throughout the basins, and in the formation
154 of E-W oriented strike-slip faults, likely related to along-strike movement on major Caledonian
155 crustal lineaments like the Great Glen and Fair Head-Clew Bay lineaments (Cooper et al,
156 2012; Le Breton et al., 2013; Anderson et al., 2018). The development of the North Atlantic
157 Igneous Province during the mid-Eocene had an impact on the Slyne and Erris basins, with
158 the intrusion of several sills and the extrusion of thick basaltic lavas of the Druid Formation
159 (Jolley & Bell, 2002). These layered basalt flows are thickest on the western margin of the
160 Southern Slyne Sub-basin, the Northern Slyne Sub-basin and in the Northern Erris Sub-basin,
161 where they degrade the quality of seismic data beneath these volcanic layers (Dancer & Pillar,
162 2001).

163

2.2. Structural Framework & Basin Morphology

165 The Slyne and Erris basins sit on the Irish Continental Shelf off the north western coast of
166 Ireland. The Irish Mainland Shelf separates the basins from the island of Ireland to the
167 southeast, while the Rockall Basin bounds the Erris Basin along its north-western margin, with
168 the Slyne and Porcupine highs bounding the Slyne Basin along its western margin (Fig. 1).
169 The Erris Ridge is a NE-SW oriented, discontinuous basement high that separates the Rockall
170 Basin from the Erris Basin and the northern Slyne Basin (Cunningham & Shannon, 1997). The
171 Porcupine Basin is located to the southwest of the Slyne Basin and separated from it by a
172 narrow basement horst.

173 The present-day morphology of the Slyne and Erris basins is largely controlled by their location
174 on the Irish Continental Shelf and the development of the neighbouring Rockall Basin; the
175 seabed above the Slyne Basin is topographically flat with no bathymetric expression, while
176 the Erris Basin dips westwards along the shelf break into the Rockall Basin. This dip is more
177 subtle in the Northern Erris Sub-basin, where the Erris Ridge is present, and more pronounced
178 in the Southern Erris Sub-basin, beyond the extent of the Erris Ridge. The Erris Basin is
179 transected by several present-day canyon systems that feed into the Rockall Basin from the
180 Irish Mainland Shelf.

181 The Slyne and Erris basins are transected by several crustal-scale structural lineaments,
182 representing suture zones and terrane boundaries separating Caledonian and Pre-Cambrian
183 basement terranes that were accreted during the Grenville and Caledonian orogenies (Chew
184 & Stillman, 2009). These structural lineaments trend NE-SW across onshore Ireland, rotating
185 to trend E-W as they continue westwards into the offshore domain (Hutton & Alsop, 1996).
186 Structural lineaments segment the younger Mesozoic rift basins, with structurally complex
187 transfer zones forming where strain is transferred from basin-bounding faults of opposed
188 polarity, with sub-basins either side of these lineaments exhibiting changes in structural style
189 and along-strike variation in their geology (Fig. 1; Trueblood, 1992; Dancer et al., 1999). The
190 Slyne Basin can be subdivided into three distinct sub-basins, the Southern, Central, and
191 Northern Slyne sub-basins, with the offshore extension of the Fair Head-Clew Bay lineament
192 separating the southern and central sub-basins (Fig. 1; Dancer et al., 1999), while the offshore
193 extension of the Great Glen Fault separates the central and northern sub-basins across a
194 complex area termed the Central Slyne Transfer Zone (CSTZ, sensu Dancer et al., 1999). The
195 Erris Basin has previously been subdivided into three sub-basins based on the predominant
196 dip of the faults in the Mesozoic section (e.g. Chapman et al., 1999); for the purposes of this
197 study the Northern and Central Erris sub-basins of previous literature have been combined.

198 3. Dataset and Methodology:

199 This study utilises an extensive, multi-vintage seismic dataset covering the majority of the
200 Slyne and Erris basins as well as extending into neighbouring regions (Fig. 3). The seismic
201 database consists of both 2D and 3D seismic reflection data. The 2D database consists of 25
202 surveys, acquired between 1975 and 2014 that total over 49,000 km in line-length. The 3D
203 database consists of 12 seismic surveys with a total area of over 6000 km², although there is
204 a significant area of overlap in the Northern Slyne Sub-basin. Most of the 3D surveys were
205 acquired between 1997 and 2003, with the 1997 Corrib 3D (Dancer & Pillar, 2001)
206 reprocessed in 2006, 2012 and 2018. Seismic quality in the Slyne and Erris basins varies from
207 very poor to good and is dependent on the near-seabed geology. Extensive Eocene volcanics
208 of the Druid Formation extruded during the formation of the North Atlantic Igneous Province,
209 as well as exceptionally hard limestones of the Upper Cretaceous Chalk Group cause
210 widespread imaging problems, principally multiple generation, energy scattering and signal
211 attenuation (Dancer & Pillar, 2001). The volcanics are thickest in the Northern Slyne Sub-
212 basin and the Southern Erris Sub-basin, as well as atop the Erris Ridge, while the Chalk Group
213 is present throughout the Erris Basin and in the Northern Slyne Sub-basin. Seismic sections
214 are presented in European polarity (Brown, 2001), where a positive downwards increase in
215 acoustic impedance corresponds to a positive (red) reflection event and a decrease
216 corresponds to a negative (blue) reflection event.

217 The seismic database was tied to released exploration and production wells and shallow
218 boreholes across the study area. To date, two exploration wells have been drilled in the Erris
219 Basin (19/5-1 and 12/13-1A), while eight exploration wells have been drilled in the Slyne Basin;
220 these include the 18/20-1 Corrib gas discovery well, in addition to four near-field exploration
221 wells in the Northern Slyne Sub-basin (19/8-1, 19/11-1A, 18/20-7, 18/25-2), with a further three
222 exploration wells drilled in the Central Slyne Sub-basin (27/4-1, 27/5-1, 27/13-1). In addition
223 to exploration wells, seven appraisal and production wells from the Corrib gas field are also
224 incorporated into this study. Of these, the 27/13-1 well terminated in the Lower Jurassic, five
225 wells penetrated the Permian (12/13-1A, 19/5-1, 19/8-1, 18/25-2, and 27/5-1), with the
226 remainder terminating in the Lower Triassic.

227 Exploration wells from neighbouring basins were also included to assess the distribution of
228 salt beyond the boundaries of the Slyne and Erris basins; these include the 12/2-1z and 12/2-
229 2 wells from the Rockall Basin, the 13/3-1 and 13/12-1 wells from the Donegal Basin, and the
230 26/22-1A, 26/21-1, 26/30-1 and 35/19-1A wells from the Porcupine Basin. The well database
231 is supplemented by three shallow boreholes; a single shallow borehole (11/20-sb01) drilled
232 on the crest of the Erris Ridge (Haughton et al., 2005), and two shallow boreholes (19/13-sb01

233 and 27/24-sb01) drilled in the Northern and Southern Slyne sub-basins respectively (Fugro,
234 1994). Data from the deep exploration wells include full suites of wireline logs (caliper, gamma,
235 density, neutron-porosity, resistivity, sonic), biostratigraphically-constrained formation tops,
236 cuttings descriptions, core photos, and time-depth relationships in the form of checkshots or
237 vertical seismic profiles (VSPs). The shallow borehole data include lithological descriptions,
238 formation tops, core photos, and select geochemical and geotechnical samples.

239 Evaporites in both the Late Triassic and Late Permian sections were identified using a
240 combination of wireline log data, cutting observations taken from both well completion reports
241 and composite logs, and core data, where available. With the relatively limited well database
242 available in the Slyne and Erris basins, the Permian and Late Triassic sections were sub-
243 divided simply; the Permian section was divided into three categories based on the proportion
244 of salt encountered, these being salt-dominated, transitional and clastic-dominated. Salt-
245 dominated sections are composed overwhelmingly of salt lithologies such as halite and
246 anhydrite, while clastic-dominated sections contain only sub-metre stringers of salt lithologies
247 in a background of sandstones, mudstones and carbonates. The transitional category contains
248 salt beds greater than a metre in thickness in a section largely composed of clastic and
249 carbonate lithologies. Stratigraphic sub-division has already been established for the Late
250 Triassic section, this being the presence or absence of the Uilleann Halite Member within the
251 Currach Formation (Fig. 2).

252 Seismic reflection data were used to map the extent of salt beyond areas where it has been
253 proven in borehole data. Where halite is present in sufficient quantities it mechanically
254 detaches sub- and supra-salt sections, forming distinct décollement surfaces on seismic
255 sections. Mobile halite also produces distinct structures including salt rollers, pillows and
256 diapirs which can be used to indicate the presence of halite in the section of interest (sensu
257 Hudec & Jackson, 2007). Detailed seismic interpretation throughout the Slyne and Erris basins
258 alongside identification of salt-related structures therefore provided a framework for mapping
259 the distribution of both Permian and Triassic salt intervals within the study area.

260

261 4. Salt Distribution and Composition:

262 Two layers of salt have been identified in the Slyne and Erris basins; the Zechstein Group,
263 and the Uilleann Halite Member within the Currach Formation. As well penetrations are
264 relatively limited in the Slyne and Erris basins, seismic character was used to constrain the
265 composition of salt-prone intervals away from areas with well-control.

266 4.1. Zechstein Group

267 The Upper Permian Zechstein Supergroup is a large and widely studied 'salt giant' present
268 across north-western Europe (Coward, 1995; Stewart, 2007; Duffy et al., 2013; Jackson &
269 Stewart, 2017). This salt body formed through the ingress and subsequent evaporation of
270 marine waters from the Boreal Ocean to the north (McKie, 2017). The North Sea rift systems
271 such as the Viking Graben provided the route through which marine waters flowed
272 southwards, while possible pathways connecting the Irish Atlantic margin and the Boreal
273 Ocean include the Faroe-Shetland Basin, the Hebridean basins, and an incipient Rockall rift
274 system (Štolfová & Shannon, 2009; McKie & Shannon, 2011; McKie, 2017).

275 The Zechstein Group has been proven in all five exploration wells that penetrate the pre-
276 Triassic section in the Slyne and Erris basins (12/13-1A, 19/5-1, 19/8-1, 18/25-2, 27/5-1), with
277 variable lithologies encountered (Fig. 4). In the 12/13-1A in the Northern Erris Sub-basin, the
278 Zechstein Group was largely composed of dolomite and anhydritic siltstones, with centimetre-
279 scale stringers of anhydrite encountered throughout the section and reported from sidewall
280 cores (Amoco, 1979). The Zechstein Group encountered in the 19/5-1 well in the Southern
281 Erris Sub-basin and the 19/8-1 well in the Northern Slyne Sub-basin consisted of interbedded
282 brown-red-grey mudstones and grey, microcrystalline dolomite accompanied by metre-scale
283 stringers of anhydrite. In the 18/25-2 well in the Northern Slyne Sub-basin, the Zechstein is
284 composed of massive anhydrite alongside thin layers of microcrystalline dolomite and
285 limestone at the top of the section, and thin layers of red-black shale towards the base of the
286 sequence. In the 27/5-1 well in the Central Slyne Sub-basin over 150 metres of massive halite
287 was encountered, with thin magnesium salts encountered at the top of the section and
288 interbedded anhydrite and claystone present towards the base of the section. A 21-metre core
289 was cut in the halite-prone section in the 27/5-1 well, described as white-pink-orange brittle
290 halite (Fig. 4). These five well penetrations indicate a broad southward increase in the salt
291 content of the Zechstein Group in the Slyne and Erris basins. Sediments belonging to the
292 Zechstein Group may have been encountered at the base of certain appraisal and production
293 wells from the Corrib gas field; a mudstone-dominated section with minor anhydrite is present
294 at the base of the Corrib Sandstone Formation in the 18/20-4 and 18/25-3 wells. However, as

295 these intervals are biostratigraphically barren (P. Copestake, pers. comm.) this remains
296 unproven.

297 The variation in lithology of the Zechstein Group creates distinct wireline log profiles for both
298 the salt-dominated and salt-poor forms (Fig. 4), with the salt-dominated sections having a
299 characteristic blocky profile with low gamma ray values and high sonic velocities, while the
300 interbedded nature of the mudstone and limestone prone sections produces a more typical
301 serrated wireline log character, higher gamma ray values and slower sonic velocities.

302 When imaged on seismic data, the Zechstein Group salt is often characterised by a distinct
303 negative impedance (blue) 'top-salt' reflector, while the unit itself is characterised by low-
304 amplitude, bedded to chaotic reflectors. Local high-amplitude reflectors are occasionally
305 observed and may represent clastic or carbonate bodies interbedded within halite-dominated
306 areas, although none of these high-amplitude bodies have been drilled to date. In areas of
307 thinner, clastic-dominated Zechstein Group facies, the Permian section is often only
308 represented by a single seismic wavelet (e.g. 19/5-1 well and seismic wavelet comparison in
309 Figure 4).

310 Well penetrations and seismic data suggest the proportion of salt within the Zechstein Group
311 decreases northwards, with only sub-metre scale stringers of anhydrite present in the 12/13-
312 1A well, the most northerly in the basin (Fig. 1, 4). Seismic data from the undrilled Southern
313 Erris Sub-basin suggests the presence of a salt-prone Permian section, where a distinct
314 detachment surface is observed beneath the Triassic section.

315 4.2. Currach Formation & Uilleann Halite Member

316 The Upper Triassic Currach Formation is the lateral equivalent to the Mercia Mudstone Group
317 of the UK, the Haisborough Group of the North Sea and the Keuper Group of Central Europe.
318 The Currach Formation has been encountered in every well in the Slyne and Erris basins,
319 except the 18/25-2 well where the Upper Triassic was faulted out. The formation consists
320 predominantly of red mudstone, locally accompanied by minor siltstone, limestone, dolomite
321 and anhydrite. Towards the base of the formation, a series of metre-scale halite beds are
322 present. In the Northern Slyne and Southern Erris sub-basins, a halite-dominated section is
323 developed at the base of the Currach Formation, termed the Uilleann Halite Member, which is
324 a brittle, crystalline white to pinkish grey halite (Enterprise, 1996). The sediments of the
325 Currach Formation represent the arid lacustrine and sabkha conditions present in the Slyne
326 and Erris basins during the Early Triassic, while the locally occurring Uilleann Halite Member
327 is indicative of a marine-influenced coastal sabkha environment during the Middle to Early
328 Triassic in the Northern Slyne and Southern Erris sub-basins (Stoker et al., 2017).

329 The wireline log profiles of the Currach Formation consist of high gamma ray values and high
330 sonic velocities associated with the mudstones that make up the bulk of the formation (Fig. 5).
331 Interbedded siltstones, sandstones and carbonates typically have lower gamma ray values
332 and slightly slower sonic velocities. The Uilleann Halite Member and smaller halite beds at the
333 base of the Currach Formation have very low gamma ray values and high sonic velocities,
334 producing blocky wireline log profiles (Fig. 5).

335 The top of the Currach Formation is marked by a high-amplitude soft or blue reflector on
336 seismic data while the base of the formation is marked by a hard or red reflector representing
337 the contact with the underlying Corrib Sandstone Formation. The Currach Formation has a
338 predominantly low-amplitude and chaotic seismic facies, with no clear distinction on seismic
339 data with the Uilleann Halite Member.

340 Well data suggests the Uilleann Halite Member is restricted to the Northern Slyne Sub-basin.
341 While the Currach Formation has been proven in every well except 18/25-2 for reasons
342 described above. The Uilleann Halite Member has been proven in the wells associated with
343 the Corrib gas field (blocks 18/20 and 18/25) in addition to 18/20-7, 19/11-1A and 19/8-1. No
344 salt is present in the Currach Formation in either of the 12/13-1A and 19/5-1 wells on the
345 margins of the Erris Basin, while only very minor stringers of anhydrite were encountered in
346 the 27/5-1 and 27/4-1 wells in the Central Slyne Sub-basin. The 27/13-1 well terminated at the
347 base of the Lower Jurassic section, while the 27/24-sb02 shallow borehole in the Southern
348 Slyne Sub-basin encountered sub-metre beds of gypsum towards the base of the Currach
349 Formation (Fugro, 1994). Seismic data from the Southern Erris Sub-basin suggests the
350 Uilleann Halite Member extends northwards into this part of the basin, with two detachment
351 surfaces visible; the lower detachment occurring on the salt of the Zechstein Group, while the
352 upper detachment occurs within the Uilleann Halite Member.

353 4.3. Other salt-prone intervals in the Slyne & Erris basins

354 In addition to the Permian and Triassic salt present in the Slyne and Erris basins, there are
355 several metres of anhydrite interbedded with the sandstones, mudstones and limestones of
356 the Hettangian to Sinemurian-aged Meelagh Formation. This anhydrite is developed in the
357 Northern and Central Slyne sub-basins, with beds up to 20 metres thick encountered
358 throughout the Meelagh Formation in the 18/20-1 well, but decreases northwards from here,
359 with no salt observed in the 19/11-1A well and only sub-metre-scale anhydrite stringers
360 recorded in the 19/8-1 well in the Northern Slyne Sub-basin, as well as the 19/5-1 and 12/13-
361 1A wells in the Erris Basin. The Meelagh Formation was deposited in an arid climate (IS16/04
362 Technical Report, 2019), with the rapid vertical variation in facies representing an unstable

363 and variable marginal marine to marine environment. Like the salt-prone intervals in the
364 Zechstein Group and Uilleann Halite Member, the anhydrite beds within the Meelagh
365 Formation have very low gamma-ray values and high sonic velocities on wireline logs. There
366 is no evidence of mechanical detachment occurring on the anhydrite beds of the Meelagh
367 Formation in seismic sections from the Slyne and Erris basins, although it is possible that
368 local, sub-seismic bed-parallel slip has occurred where these evaporites are present.

369 Within the Visean section of the 19/5-1 well in the Erris Basin, a sidewall core and cuttings at
370 2141 metres Measured Depth (mMD) are described as claystones containing stringers of
371 white anhydrite (Amoco, 1978). Gypsum has been encountered onshore Ireland in the
372 equivalent section in the Lough Allen Basin (Ambassador, 1962; Grennan, 1992). While this
373 section was only reached in a single well in the Erris Basin and beyond the scope of this study,
374 it indicates the presence of salt-prone strata at four discrete stratigraphic levels
375 (Carboniferous, Upper Permian, Upper Triassic, and Lower Jurassic) in the Slyne and Erris
376 basins.

377 5. Salt structures in the Slyne and Erris basins

378 In areas of sparse well control, evidence of salt-related structures is supported by the
379 identification of characteristic features on seismic data. The distribution and types of salt
380 structures observed within the Slyne and Erris basins varies significantly between different
381 sub-basins. This section analyses several of these structures and their implications for
382 understanding salt composition and distribution.

383 5.1. Southern and Central Slyne Sub-basins

384 In the south of the study area only the Zechstein Group is salt prone, while the Uilleann Halite
385 Member is not developed within the Currach Formation. In this area the Zechstein Group acts
386 as a significant décollement between the pre-salt Palaeozoic basement and the post-salt
387 Mesozoic section. The Southern and Central Slyne sub-basins are two contiguous half-graben
388 which dip steeply westwards towards the basin-bounding fault running along their western
389 margins, across which they are downthrown relative to the Porcupine High. The Central Slyne
390 Sub-basin is downthrown relative to the Southern Slyne Sub-basin across the offshore
391 extension of the Highland Boundary-Fair Head Clew Bay Lineament (Fig. 1).

392 In the Southern Slyne Sub-basin, a single, relatively large salt roller is identified in the centre
393 of the sub-basin (Fig. 6). The Triassic, Lower Jurassic and Middle Jurassic sections dip more
394 steeply north-westwards than both the underlying Carboniferous basement and the overlying
395 Upper Jurassic section, with the Base Upper Jurassic Unconformity eroding the crest of the
396 structure.

397 The Central Slyne Sub-basin is a westward-dipping half-graben composed of a series of ramp-
398 syncline basins (Fig. 1, 7). It also likely represents the erosional remnants of a significantly
399 wider basin that included the Slyne Embayment and a smaller disconnected half-graben to
400 the west of the Central Slyne Sub-basin (Fig. 1, 7A). The Slyne Embayment has a similar
401 sedimentary fill to that of the Central Slyne Sub-basin, with the Triassic and Jurassic sections
402 overlying a salt-prone Zechstein Group (Fig. 7A). In addition, westward dipping listric faults
403 that detach into the Zechstein salt observed in the Central Slyne Sub-basin and down-dip
404 compression recorded in the Slyne Embayment may suggest that these are components of
405 linked gravitational system. These observations are consistent with a predominately Late
406 Jurassic age for the major fault along the western margin of the Central Slyne Sub-basin.
407 Kilometre-scale erosion of the Jurassic sedimentary section during the Cretaceous and
408 Cenozoic (Dancer et al., 1999; Biancotto et al., 2007) would have isolated the Slyne
409 Embayment from the Central Slyne Sub-basin by removing the footwall of the intervening fault

410 to create the Slyne High (Fig. 7A). The emergence of the basin-bounding fault during Late
411 Jurassic extension would have acted as a barrier to linked gravitational system between the
412 Central Slyne Sub-basin and Slyne Embayment, resulting in the ramp-syncline geometry
413 observed at present.

414 A notable feature in the Central Slyne Sub-basin is the presence of several high-relief, broadly
415 anticlinal structures in the immediate hanging-wall of the bounding fault along the western
416 margin of the basin (Fig. 7). While ostensibly similar, each structure exhibits subtle variations
417 in geometry and composition. The Triassic to Middle Jurassic section penetrated in the 27/4-
418 1 well in the immediate hanging-wall of the bounding fault was encountered at similar depths
419 in the 27/5-1 well on the eastern margin of the Central Slyne Sub-basin (Fig. 7A). The Upper
420 Jurassic section onlaps the steeply dipping eastern flank of the 27/4-1 structure and thickens
421 eastwards into the hanging-wall of a major listric fault. Movement on this listric fault likely
422 facilitated the formation of the 27/4-1 structure, creating the accommodation space for the
423 Upper Jurassic growth sequences, giving an indication of timing of both fault movement and
424 the formation of the 27/4-1 structure.

425 The southern-most hanging-wall structure (Fig. 7B) is another high-relief anticlinal closure,
426 with the Lower and Middle Jurassic section adjacent to the bounding-fault at a similar depth
427 to the same section on the eastern margin of the basin. There is a distinct rotation of the Lower
428 and Middle Jurassic section facilitated by a detachment surface above the Triassic, indicating
429 the Uilleann Halite Member may be developed within the Currach Formation at this location
430 and acted as a mechanical detachment during extension.

431 Between these two high-relief structures there is a relative saddle abutting the basin-bounding
432 fault, forming a gently dipping dome. A distinct angular unconformity is observed beneath the
433 Upper Jurassic section (Fig. 7C) which is not observed at the crests of the structures along-
434 strike (Fig. 7A & B). Correlation from the 27/4-1 well indicates that the Middle Jurassic Kite
435 Group and a significant portion of the Lower Jurassic Lias Group, down to the Pabay
436 Formation, are absent from the crest of this saddle (Fig. 7C), while being preserved along-
437 strike at the higher relief 27/4-1 location (Fig. 7A). This indicates that this location was at a
438 higher relief relative to the present-day high-relief structures to the north and south during the
439 period of uplift and erosion that preceded Oxfordian rifting. This elevated area was likely to
440 have been cored by a gentle salt pillow before the emergence of the basin-bounding fault. As
441 the main phase of rifting initiated during the Oxfordian, the structures to the north and south
442 of this small salt pillow began to form, evidenced by onlap onto their flanks by the Upper
443 Jurassic section in this part of the basin.

444 Similar to the structure in Fig. 7C, a significant section of the Middle and Lower Jurassic
445 stratigraphy has been eroded from the eastern margin of the Central Slyne Sub-basin. The
446 Kite Group and part of the Lias Group, down to the Pabal Formation, are absent beneath the
447 base-Upper Jurassic unconformity in the 27/5-1 well while being present in the 27/4-1 well
448 (Fig. 7A). The base-Upper Jurassic unconformity is encountered at a relatively similar depth
449 present-day in both wells, 700 mMD and 845 mMD respectively (IS16/04 Technical Report,
450 2019), while having significantly different subcrops, highlighting the variation in Zechstein
451 Group salt topography during different extensional episodes.

452 5.2. Northern Slyne Sub-basin

453 Several salt-cored folds are observed in the Northern Slyne Sub-basin, typically oriented NE-
454 SW and NNE-SSW, parallel to the syn-rift faults. Composed of Zechstein salt, these pillows
455 are between 5 to 15 kilometres in length and up to 10 kilometres wide, often flanked by salt
456 withdrawal synclines which likely developed by salt movement into the pillows. The folded
457 Mesozoic stratigraphy above these salt pillows has been the target of several exploration wells
458 in this part of the basin, including the 18/20-1 (Corrib), 18/20-7 and 19/11-1A wells (Fig. 8).
459 The 19/8-1 well also targeted a large fold but encountered the Corrib Sandstone Formation
460 over 2km shallower than prognosed (StatoilHydro, 2009), with the mapped structure likely to
461 represent a Variscan fold in the pre-salt Carboniferous basement.

462 Several of these salt-cored folds have large delamination faults above their crests which sole
463 out into the Uilleann Halite Member at the base of the Currach Formation. These faults trend
464 parallel to the axes of the salt-cored folds and are likely to have developed in tandem with the
465 pillows of Permian salt, representing thin-skinned gravitational failure caused by the increasing
466 relief at the apex of the folds. These delamination faults are often accompanied by the
467 formation of salt rollers in their footwalls (Fig. 8A, B), in addition to faulted rollovers in their
468 hanging-walls. The salt roller in the footwall of the delamination fault above the Corrib anticline
469 has developed further, forming a small salt diapir, with apparent onlap of the Lower Jurassic
470 section onto the western flank of the salt diapir (Fig. 8B), indicating relatively early diapir
471 growth and emergence. This is confirmed by the 18/20-6z vertical producer well from the
472 Corrib gas field, which penetrated a section of the Uilleann Halite Member over 620m thick.

473 These delamination faults have been reactivated at several different stages during the
474 Cretaceous and Cenozoic post-rift period; significant growth sequences in the Cretaceous
475 section are observed in the hanging-walls of these large delamination faults, particularly in the
476 Lower Cretaceous Spurdog Formation (Fig. 8A, B). The delamination faults also offset the top
477 of the Druid Formation lavas and a portion of the overlying Cenozoic sediments, which are

478 dated as 40-43 Ma in the 18/20-1 well (Dancer et al., 1999) and Miocene to Pleistocene
479 (IS16/04 Technical Report, 2019). The lack of folding of this Cretaceous and Cenozoic section
480 indicates the later fault movement is more likely related to continued extension on these
481 delamination faults and growth of associated reactive diapirs rather than modification of the
482 salt-cored fold.

483 5.4. Southern Erris Sub-basin

484 The Southern Erris Sub-basin dips steeply north-westward as a result of post-rift thermal
485 subsidence in the neighbouring Rockall Basin during the Cenozoic (Fig. 9-12). The western
486 margin of the Erris Basin experienced significant rift-shoulder uplift during the Cretaceous,
487 related to rifting in the Rockall Basin, with a kilometre-scale section of Jurassic stratigraphy
488 removed. This part of the Erris Basin is dominated by a series of closely spaced, westward-
489 dipping faults (Fig. 9). Previous authors had interpreted these faults as through-going
490 basement-linked structures (e.g. Shannon & Naylor, 1998; Chapman et al., 1999; Corfield et
491 al., 1999), however more modern data reveals their listric nature, with many faults detaching
492 on the Uilleann Halite Member above closely spaced salt rollers (e.g. Fig. 9). The Zechstein
493 Group also acts as a décollement in this part of the basin, mechanically detaching the Corrib
494 Sandstone Formation from the underlying Carboniferous basement. Salt pillows form in the
495 Zechstein Group and fold the overlying Corrib Sandstone Formation in a similar manner to
496 those in the Northern Slyne Sub-basin (Fig. 8)

497 More faults are through-going across the Permian section in the Southern Erris Sub-basin
498 than in the Slyne Basin, indicating that the Zechstein Group in this part of the basin may
499 contain less halite and more immobile evaporite lithologies. The proportion of salt decreases
500 towards the eastern margin of the Erris Basin, with faults being hard-linked through the
501 Mesozoic and Palaeozoic sections (Fig. 10). Only a thin layer of anhydrite was encountered
502 in the 19/5-1 well drilled on the eastern edge of the Southern Erris Sub-basin (Fig. 4).

503 5.5. Northern Erris Sub-Basin

504 The Northern Erris Sub-basin is an asymmetric graben, bounded along its eastern margin by
505 the Irish Mainland Shelf, and separated from the Rockall Basin to the west by the narrow,
506 elongate Erris Ridge. The single well (12/13-1A) drilled in this part of the basin encountered
507 only sub-metre scale stringers of anhydrite in a 19 metre-thick Zechstein Group section, while
508 no evaporite lithologies were present in the Currach or Meelagh formations. There is little
509 evidence on seismic sections to indicate the presence of significant thicknesses of salt in this

510 part of the basin, with all clearly imaged faults hard-linked through the Zechstein Group with
511 little evidence for growth sequences in the pre-Triassic sections (Fig. 11, 12).

512 There is similarly scarce evidence for salt in neighbouring areas; both wells in the Donegal
513 Basin to the northeast, 13/3-1 and 13/12-1 (Fig. 1), encountered the Pennsylvanian Blackthorn
514 Group directly beneath the Base-Cenozoic Unconformity (Texaco, 1978; Lundin, 2006), while
515 the 12/2-1 and 12/2-2 wells in the Rockall Basin to the west encountered the Triassic Cot
516 Sandstone Formation (lateral equivalent to the Corrib Sandstone Formation) and Upper
517 Jurassic Dawros Formation respectively lying directly above the Pennsylvanian Sorrel Group,
518 with no Permian, Upper Triassic or Lower Jurassic sediment encountered (IS16/04 Technical
519 Report, 2019).

520 6. Discussion:

521 6.1. Timing and drivers of halokinesis in the Slyne and 522 Erris basins

523 Understanding the timing of salt movement during basin development is important both for
524 unravelling the structural evolution and for understanding the development of the petroleum
525 system. Regional extension is recognised as a common mechanism for the initiation of salt
526 tectonics (Jackson & Vendeville, 1994; Jackson & Hudec, 2017) and is the most likely trigger
527 for halokinesis in the Slyne and Erris basins. There is evidence of halokinesis occurring at
528 several stages during basin evolution, including during both the Early to Middle Jurassic and
529 Late Jurassic phases of rifting, in addition to post-rift modification of salt structures during the
530 Cretaceous and Cenozoic.

531 In the Central Slyne Sub-basin growth sequences are observed in the Lower Jurassic section
532 in the hanging walls of small intra-basinal listric faults which sole out in the Zechstein Group
533 (Fig. 7). The faults controlling these growth sequences are then truncated by the Base Upper
534 Jurassic Unconformity, indicating discrete extension confined to the Early-Middle Jurassic.
535 Faults of a similar age are also interpreted in the Southern Erris Sub-basin, where faults which
536 sole out above rollers of Uilleann Halite are truncated by the Base Upper Jurassic
537 Unconformity. Several of these faults have hanging-wall sequences that record limited growth
538 during the Early Jurassic (Fig. 9) and were reactivated during the main phase of rifting during
539 the Late Jurassic and subsequently truncated by the Base-Cretaceous Unconformity. In the
540 Southern Slyne Sub-basin, the Triassic and Lower Jurassic section tilted above the large
541 Zechstein reactive diapir is truncated by the Base Upper Jurassic unconformity (Fig. 6),
542 indicating that inflation of the salt roller in the footwall of the fault began during the Early-Middle
543 Jurassic before the crest was eroded during the formation of the unconformity and before
544 further inflation during Late Jurassic rifting (Fig. 13). There is further evidence of halokinesis
545 in the Northern Slyne Sub-basin with subtle thinning of the Lower Jurassic section onto the
546 crest of the Corrib anticline (Fig. 8B), indicating that the Zechstein Group salt pillow was
547 creating relief during the Early Jurassic (Fig. 13).

548 The main phase of rifting in the Slyne and Erris basins, during the Late Jurassic, was preceded
549 by the formation of the regional Base Upper Jurassic Unconformity mentioned previously (Fig.
550 13). The majority of intra-basinal faulting during this time occurred as thin-skinned, basement-
551 detached deformation (Figs 6-9) apart from in the Northern Erris Sub-basin where the Uilleann
552 Halite Member is absent and the Zechstein Group is composed of carbonates and clastics

553 (Fig. 11 & 12). In the Central Slyne Sub-basin growth sequences (Fig. 7A) and onlap (Fig. 7B)
554 are observed on the flanks of the high-relief structures in the immediate hanging-wall of the
555 basin-bounding fault. Unlike other high-relief structures where distinct crestal erosion is
556 recorded at the Base Upper Jurassic Unconformity, these structures likely emerged during
557 Late Jurassic basin extension (Fig. 13). Their geometry, as well as the likely presence of salt
558 in the Slyne Embayment to the west, indicate that these structures may have formed as forced
559 folds above the active footwall of the basin-bounding fault, creating the topography for onlap
560 and growth sequences to form locally in ramp syncline basins (e.g. Withjack & Callaway, 2000;
561 Coleman et al., 2017). The observation of salt in the undrilled Slyne Embayment to the west
562 of the Central Slyne Sub-basin, in the form of folded Mesozoic sediments mechanically
563 detached from the brittle deformation in the Carboniferous basement (Fig. 7A), is further
564 support for the idea that Permian salt and the overlying Mesozoic section may have
565 overstepped the now eroded footwall of the bounding fault before kilometre-scale uplift and
566 erosion during the Cretaceous and Cenozoic (Fig. 7A).

567 Along-strike variation in these structures suggests there may be more complexity to their
568 evolution beyond a breached salt-detached monocline. Dancer et al. (1999) suggested five
569 potential mechanisms for the formation of the structure targeted by the 27/4-1 well (Fig. 7A),
570 with one being salt diapirism. Crucially, this paper predated the acquisition of good-quality 3D
571 seismic data (2000) and the drilling of the 27/4-1 well (2009), datasets which highlight the
572 modification of these structures during basin evolution. Specifically, the preservation of the
573 Middle and Lower Jurassic section proven in the 27/4-1 well, combined with the absence of
574 the Kite Group and Dun Caan Shale and Whitby Mudstone formations along-strike (Fig. 7C)
575 highlights the modification of structures during basin evolution, with the eroded crest of the
576 structure in Fig. 7C being over 600ms TWT (c. 1200m) deeper than the seemingly uneroded
577 crest of the structure in Fig. 7A. This evidence suggests there may have been a high-relief
578 salt-cored structure during the Early and Middle Jurassic at the location of Fig. 7C, possibly a
579 salt pillow or a reactive diapir similar to that imaged in Fig. 6 which exhibits comparable crestal
580 erosion, which then collapsed during the main phase of rifting in the Late Jurassic with along-
581 strike migration of the Permian salt into the present-day higher elevation structures.

582 Several salt structures in the Slyne Basin underwent significant post-rift modification during
583 the Cretaceous and Cenozoic, driven by rifting in the Rockall Basin during the Cretaceous,
584 and subsequent Cenozoic post-rift thermal subsidence, mid-Atlantic ridge-push and the
585 development of the Icelandic plume (Dancer et al., 1999). There is evidence throughout the
586 Slyne and Erris basins of fault reactivation, with several of these reactivations occurring in
587 salt-prone areas where the faults are listric and sole out in either the Zechstein Group or the
588 Uilleann Halite Member (Fig. 7 & 9). Other structures appear not to have been reactivated

589 during this post-rift activity (e.g. Fig. 6), although the lack of Cretaceous sediments in the
590 Central and Southern Slyne Sub-basins means that any fault movement during this phase of
591 post-rift deformation is not recorded. This Cretaceous and Cenozoic reactivation is subtle, with
592 movement on reactivated faults being in the order of 10s of metres, much lower than the syn-
593 rift fault offsets which are in the order of several hundred metres to kilometres in scale.

594 The seismic data analysed above indicates that there were two main phases of syn-rift
595 halokinesis in the Slyne and Erris basins; the first of these occurred during Early to Middle
596 Jurassic extension with a subsequent phase of salt movement during Late Jurassic rifting.
597 Some salt structures formed during the first phase of halokinesis were reactivated and
598 continued to grow during the Late Jurassic period of salt movement (e.g. Fig. 6, 8), while
599 others collapsed during this second phase of rifting with others forming in their stead (Fig. 7).
600 Several of these salt-related structures underwent minor modification during post-rift tectonic
601 activity in the Cretaceous and Cenozoic.

602 6.1.1. Kinematic interaction between salt layers

603 In the Northern Slyne and Southern Erris sub-basins, two distinct layers of autochthonous salt
604 are present at different stratigraphic intervals, which has previously been termed 'double-
605 decker' salt tectonics (Corcoran & Mecklenburgh, 2005). In these areas a clear relationship
606 between the timing of halokinesis in each layer can be observed. The most well imaged of
607 these is the structure containing the Corrib gas accumulation, where two discrete salt-related
608 structures are visible: a Zechstein Group salt pillow and an Uilleann Halite Member diapir (Fig.
609 8B). These structures have parallel trends, oriented NE-SW (Fig. 14). The Uilleann Halite
610 diapir has a distinct pointed crest, indicating it is likely to be a reactive diapir which formed
611 during delamination faulting of the Jurassic overburden during the growth of the Zechstein salt
612 pillow at depth; as the Zechstein salt pillow grew and folded the overlying Triassic and Jurassic
613 section, listric delamination faults began to form in the Jurassic section on the crest of the fold,
614 with these faults soling out in the Uilleann Halite (Fig. 13). The throw on these delamination
615 faults is greatest at the apex of the Zechstein salt pillow and resultant Lower Triassic fold,
616 facilitating inflation in the footwall with Uilleann Halite and leading to the reactive diapir sitting
617 parallel to the fold axis of the salt pillow (Fig. 14A, B). Similar structures are observed above
618 other Zechstein salt pillows in the Northern Slyne Sub-basin (e.g. Fig 8A).

619 While the Zechstein salt pillow controlled the initial evolution of the Uilleann Halite diapir, the
620 subsequent growth of this diapir during continued extension may have in turn influenced the
621 development of the salt pillow. As regional extension continued, particularly during the Late
622 Jurassic, the delamination fault above the Corrib anticline experienced further normal

623 movement. This fault movement displaced the overburden section downwards off the crest of
624 the anticline, creating thicker sedimentary sections in the flanking synclines (Fig. 8B) while
625 reducing the sediment thickness at the apex of the fold. These thicker sedimentary sections
626 on the flanks of the anticline would then inflate the Zechstein salt pillow further through
627 differential loading, creating a steeper structure which would then lead to further movement
628 on the crestal delamination fault. The delamination fault above the Corrib gas field was
629 reactivated again during the Cretaceous and the Cenozoic, with distinct growth sequences
630 observed in the Cretaceous section in the immediate hanging-wall of the delamination fault
631 (Fig. 8B), which also offsets the top of the Druid Formation volcanics. This volcanic sequence
632 is dated between 54.3 and 40 Ma (early-mid Eocene) in the 18/20-1 well and the 19/13-sb02
633 shallow borehole in the Northern Slyne Sub-basin (Fugro, 1994; Corcoran & Mecklenburgh,
634 2005), indicating how recently this Permian-Triassic salt relationship was active. A similar
635 relationship likely drove the syn- and post-rift evolution of other salt pillow and diapir pairs
636 observed in the Northern Slyne and Southern Erris sub-basins (e.g. Fig. 8A, 9).

637 Previous structural models for the Corrib structure (e.g. Corcoran & Mecklenburgh, 2005;
638 Dancer et al., 2005) have suggested a polarity reversal in the delamination fault at different
639 stages of basin evolution, with an initial westward-dipping fault plane during the Early Jurassic
640 changing to the dominant eastward-dipping fault observed today during the Late Jurassic. A
641 thinner Lower and Middle Jurassic section encountered on the eastern flank of the anticline
642 was interpreted as the eroded footwall of the westward-dipping fault relative to the thicker
643 section observed on the western flank (Fig. 8B). Recent biostratigraphic analysis has revealed
644 that complete Lias Group and Kite Group sections have been encountered in all wells drilled
645 in the Corrib gas field, with an attenuated but complete section encountered in the Lower and
646 Middle Jurassic on the eastern flank of the anticline (IS16/04 Technical Report, 2019). This
647 attenuated section was likely deposited on the crest of a salt-cored fold during the Early and
648 Middle Jurassic and is commonly observed above salt pillows (Jackson & Hudec, 2017).
649 During Late Jurassic extension significant heave on the delamination fault moved the
650 attenuated crestal section of Lower and Middle Jurassic sediments eastwards down the flank
651 of the anticline.

652 The kinematic interaction of stratigraphically discrete salt layers observed in the Slyne & Erris
653 basins may act as a structural template for similar stratigraphic configurations in other basins
654 (Fig. 13). Examples include the Sole Pit Basin and Danish Central Graben in the North Sea,
655 where delamination faults sole out in the Triassic Muschelkalk Halite above Zechstein Group
656 salt pillows (Glennie, 1997; Hansen et al., 2020).

657

6.1.2. Relationship between timing of halokinesis and the petroleum system

658

659 The timing of formation and subsequent modification of the Corrib structure played a crucial
660 role in both the success and failure of the 18/20-1 discovery well. The well was drilled to the
661 northwest of the main delamination fault, passing through the tilted fault block above the
662 Uilleann Halite diapir (Fig. 8B, 14C). The well encountered oil-stained sandstones throughout
663 the Upper Jurassic section (Enterprise, 1996; Dancer et al., 2005), evidence of a breached
664 paleo-accumulation, before discovering the gas accumulation in the Corrib Sandstone
665 Formation, sealed by the Uilleann Halite Member. Post-rift movement on the main
666 delamination fault bounding the Jurassic structural trap (Fig. 14C) during both the Cretaceous
667 (Fig. 14D) and Cenozoic (Fig. 8B) post-dates the main phase of hydrocarbon generation and
668 migration at the end of the Jurassic (Petroleum Affairs Division, 2005). This late movement on
669 the delamination fault likely caused cross-fault juxtaposition of Upper Jurassic sandstones,
670 possible dilation of the fault plane and breaching of the top seal, leading to the loss of the oil
671 accumulation. However, since the delamination fault soles out in the Uilleann Halite Member
672 this post-charge fault movement did not interact with the Corrib Sandstone Formation and the
673 gas accumulation.

674 Similarly, post-rift modification of the underlying Zechstein Group salt pillow may explain the
675 nature of the Corrib anticlinal trap; the anticline is significantly underfilled, with potential
676 associated mechanisms including the presence of a small leaking fault at the current gas-
677 water contact or leakage through the sealing Uilleann Halite Member during Cretaceous and
678 Cenozoic exhumation (Corcoran & Doré, 2002; Corcoran & Mecklenburgh, 2005). The modest
679 overpressure within the reservoir section (Corcoran & Doré, 2002) and halite composition of
680 the top-seal indicate that the original charge pre-dating exhumation is preserved and that
681 leakage without clear evidence of salt-welding is difficult. Salt tectonics may instead be
682 responsible for the underfilled nature of the Corrib anticline, with post-rift movement on the
683 delamination fault and growth of the Uilleann Halite Member diapir perhaps driven by post-rift
684 growth of the Zechstein Group salt pillow. Additional post-rift (and post-charge) growth of this
685 salt pillow would have increased the vertical relief and cross-sectional area of the anticline and
686 the corresponding volume of the structural trap beyond that filled by gas during the Late
687 Jurassic and Early Cretaceous. This highlights the multiphase evolution of this and probably
688 other structures within the Slyne and Erris basins and how understanding their structural
689 history will be critical to improving exploration success in the future.

690 6.2. The Slyne and Erris basins in context with other salt- 691 prone basins of the North Atlantic

692 Results presented thus far have highlighted the importance of salt during the structural
693 evolution of the Slyne and Erris basins and defined a range of structures that are characteristic
694 of salt-involved deformation in this area. These findings can, by analogy, be used to delimit
695 the occurrence of salt in neighbouring basins where the lack of well data has made
696 interpretation of salt more speculative. A more detailed understanding of salt distribution can
697 in turn be used to refine paleogeographic models for the Late Permian and Late Triassic of
698 the Irish Atlantic margin.

699 6.2.1. Irish Atlantic Margin

700 No Permian rocks have been encountered outside of the Slyne and Erris basins on the Irish
701 Atlantic margin to date, although Permian ages have been suggested for a sandstone section
702 encountered above the Carboniferous in the 12/2-1 and 12/2-2 wells on the eastern margin of
703 the Rockall Basin, adjacent to the northern Erris Basin (Shell, 2009; Tyrrell et al., 2010).
704 Conversely, Early and Late Triassic-aged sections have been proven in several basins,
705 including the Porcupine and Celtic Sea basins.

706 In the Porcupine Basin metre-scale anhydrite layers were encountered towards the top of the
707 Currach Formation in well 26/22-1A (BP, 1979), while the 35/19-1A well encountered 24m of
708 allochthonous salt spread over two intervals intruded into Upper Jurassic sediments on the
709 eastern margin of the Porcupine Basin (Britoil, 1986). In this well the salt is composed of
710 massive halite with thin slivers of red mudstone likely representing rafted sections of Currach
711 Formation mudstones, suggestive of Upper Triassic salt, equivalent to the Uilleann Halite
712 Member in the Slyne and Erris basins. As an Uilleann Halite Member equivalent has not been
713 encountered in the northern Porcupine Basin to date, this Triassic salt is likely to have
714 migrated from a more central, undrilled part of the basin to the south.

715 The Goban Spur Basin, along the southern margin of the Porcupine Basin, may also contain
716 Triassic salt, with evidence on seismic data of décollement surfaces and salt pillows beneath
717 the Base-Cretaceous Unconformity (Fig. 15). A pronounced fold occurring above near-
718 horizontal, unfolded reflectors (Fig. 15) is interpreted as local Lower Triassic sediments
719 deposited within the Variscan fold and thrust belt but since the single well drilled in the Goban
720 Spur Basin terminated in Hettangian sediments, this interpretation remains speculation (Colin
721 et al., 1992).

722 Previous authors have noted décollement surfaces in the perched basins along the margins
723 of the Irish sector of the Rockall Basin, including the Bróna and Fursa basins on the eastern
724 margin (Thomson & McWilliam, 2001; Štolfova & Shannon, 2009) and the Conall and Rónán
725 basins on the north-western margin (Corfield et al., 1999; Walsh et al., 1999). Distinct
726 detachment horizons are visible on seismic data from these basins, with faults observed soling
727 out in these horizons. In the Rónán Basin on the western margin of the Rockall Basin, a subtle
728 décollement is visible within the steeply dipping reflectors, mechanically detaching faults
729 above and below it, with a distinct local thickening along the south-eastern margin of the basin
730 interpreted as a salt pillow (Fig. 16A). Similarly, two distinct sets of faults are observed either
731 side of a décollement in the Fursa Basin (Fig. 16B). While these basins are undrilled at
732 present, these décollement surfaces likely represent lateral equivalents to Permian salt proven
733 in the Slyne Basin, as interpreted by Štolfova & Shannon (2009). In these basins this layer of
734 salt plays a similar role in mechanically detaching the Mesozoic basin fill, which displays
735 similar seismic facies to those observed in the Slyne and Erris basins, from the Palaeozoic
736 basement.

737 6.2.2. Neighbouring basins on the European Atlantic 738 margin

739 The basins of the Irish Atlantic margin belong to a chain of basins that extend along the
740 European Atlantic margin, many of which also contain significant salt deposits that correlate
741 with those proven in the Slyne and Erris basins. Directly north of the study area are a series
742 of interconnected basins off the north-western coast of the UK which contain significant
743 thicknesses of sediments defined broadly as Permo-Triassic due to the relative lack of
744 biostratigraphic control (Steel & Wilson, 1975; Hitchen et al., 1995). Both wells drilled in the
745 West Orkney Basin encountered several hundred metres of halite interbedded with
746 sandstones and mudstones with anhydrite stringers belonging to the West Orkney Evaporite
747 Formation interpreted as being Permian in age and representing Zechstein Group equivalents
748 (Elf, 1991; Hitchen et al., 1995; McKie, 2017). Along-strike in the West Shetland Basin the
749 205/27a-1 well encountered interbedded Upper Permian sandstones and mudstones with
750 anhydrite stringers (Hitchen et al., 1995). There is little evidence of salt in the Upper Triassic
751 section in this region, instead being dominated by sandstone (Swiecicki *et al.* 1995).

752
753
754
755
756
757
758
759
760
761
762
763
764
765
766
767
768
769
770
771
772
773
774
775
776
777
778
779
780
781
782
783
784
785
786

6.2.3. Implications for the Permian & Triassic paleogeography of the Irish Atlantic margin

Paleogeographic reconstructions of north-western Europe during the Permian and Triassic often present the Irish Atlantic margin in simplified terms at the fringes of regional maps, owing to the relative lack of well penetrations and published data when compared with neighbouring regions. The Early Triassic is an exception, due to its significance in the petroleum system of the Corrib gas field (Dancer et al., 2005), with a relatively well understood paleogeography in which the Slyne and Erris basins are host to southwards-verging braided fluvial systems (e.g. Tyrell et al., 2007; McKie & Williams, 2009; Franklin et al., 2019), while no Early Permian rocks have been encountered on the Irish Atlantic margin to date. Existing paleogeographic reconstructions (e.g. Doré, 1991; Knott et al., 1993; McKie & Shannon, 2011; McKie, 2017; Scotese & Schettino, 2017) present the Irish Atlantic margin as the terminus of tortuous seaways that extended into the Pangean supercontinent; During the Late Permian ingress of marine waters came from the Boreal Ocean to the north through the West of Shetland region, but during the Late Triassic a seaway extended from the Tethys Ocean to the southeast across Central and Western Europe to reach Ireland through the Cheshire Basin in the UK. Using the results presented in this study as well as the speculative interpretations of neighbouring regions discussed above, it is possible to refine existing paleogeographic models of the region during the Late Permian and Late Triassic, and include the basin-specific detail for the Irish Atlantic margin that was absent in previous regional syntheses.

The distribution of Late Permian salt of both the UK and Norwegian North Sea has been interpreted to be fault controlled, with salt-prone lithologies deposited in the hanging walls of active faults, while marginal carbonate and siliciclastic facies accumulated on basin margins and intra-basinal highs. The exact age of faulting remains ambiguous, with the Late Permian bathymetry either being inherited from Early Permian rifting, or representing syn-depositional extension in the Late Permian (e.g. McKie & Shannon, 2011; Jackson & Lewis, 2016; Jackson et al., 2019). Applying a similar model to the Slyne and Erris basins, the thicker salt-prone Zechstein Group in the Slyne Basin and the Southern Erris Sub-basin would be indicative of active Permian faulting, while the presence of thin marginal deposits in the Northern Erris Sub-basin suggests this area was a relative high with little active faulting. Therefore, the marine pathway connecting the Slyne Basin to the Boreal Ocean likely traversed an area other than the Erris Basin, an interpretation supported by the lack of Permian sediments in the north-eastern Irish Rockall Basin, the Donegal Basin and the Sea of the Hebrides Basin. The layers of salt interpreted in the Rónán Basin, the pre-Cretaceous 'conjugate margin' to the Erris Basin (Fig. 16A), might therefore indicate that the route of active Permian rifting may have been an

787 anastomosing series of rifts extending northwards along the axis of a proto-Rockall and West
788 of Shetland rift system, with remnants of these basins occupying the margins of the Rockall
789 Basin after rifting and hyperextension in the Cretaceous (Fig. 17A). This may indicate that the
790 framework for the present-day configuration of rift basins on the Irish Atlantic margin may have
791 been established in-part during this period of Permian extension.

792 During the Late Triassic, the Northern Slyne and Southern Erris sub-basins may have also
793 been the terminus for a seaway, this time stretching from the Tethys Ocean to the southwest.
794 The Uilleann Halite Member in the Northern Slyne and Southern Erris sub-basins (Fig. 1, 5)
795 likely represents the deposits of incursions of marine brines from the southwest. In
796 neighbouring regions such as the Ulster Basin and the Irish Sea basins several discrete layers
797 of halite are interpreted as successive marine flooding events into these regions (Jackson &
798 Mulholland, 1993; Dunford et al., 2001; McKie, 2017). The Uilleann Halite Member might
799 therefore represent the deposits of a more extensive marine incursion that extended beyond
800 those found in the Irish Sea and North Channel region. The exact route of marine ingress is
801 uncertain and likely obscured by Cretaceous and Cenozoic erosion, but may have come from
802 the south, through the Celtic Sea and Porcupine basins (e.g. Scotese & Schettino, 2017), or
803 from the north or east through the Donegal Basin or the Ulster-Larne Basin (e.g. Naylor, 1992).
804 The paleogeography of the Late Triassic salt layers is distinct from the Late Permian as these
805 marine incursions intrude into a predominantly arid lacustrine environment, represented by
806 the thick red mudstones which dominate the majority of the Currach Formation (Fig. 5), which
807 differs from the predominantly marine environment of the Zechstein Group deposits,
808 represented by cleaner halite with few mudstone inclusions (Fig. 4). Additionally, the Triassic
809 was a period of tectonic quiescence on the Irish Atlantic margin following Permian rifting (e.g.
810 Tyrrell et al., 2007; Franklin et al., 2019) and Late Triassic sediments likely spilled out beyond
811 the present-day basin boundaries (Fig. 17B), with their present-day distribution a product of
812 preservation in post-Triassic rift basins.

813 7. Conclusions

814 Using a combination of 2D and 3D seismic, wireline, and core data, this study investigated the
815 distribution of the salt in the Slyne and Erris basins and its influence on the structural evolution
816 of these basins.

- 817 1. Two main salt-prone intervals are present in the Slyne and Erris basins: The Upper
818 Permian Zechstein Group and the Upper Triassic Uilleann Halite Member of the Currach
819 Formation. The Zechstein Group is salt prone throughout the Slyne Basin and in the
820 Southern Erris Sub-basin, becoming dominated by carbonates and clastics in the
821 Northern Erris Sub-basin. The Uilleann Halite Member is developed in the Northern
822 Slyne Basin and Southern Erris sub-basins.
- 823 2. Salt acts as a décollement and mechanically detaches distinct sections of stratigraphy
824 within the Slyne and Erris basins. The Zechstein Group has the largest impact on basin
825 development and is a regional décollement surface, with most syn-rift normal faults
826 detached from the pre-Permian basement along this surface. The Uilleann Halite
827 Member exerts similar controls on basin development where it is present.
- 828 3. Halokinesis occurred at several stages during the evolution of the Slyne and Erris
829 basins. This includes extension in the Early Jurassic and the Late Jurassic, as well as
830 post-rift reactivation during the Cretaceous and Cenozoic. This salt movement has
831 created a variety of relatively immature salt-related structures throughout the Slyne
832 and Erris basins, including salt pillows, rollers and reactive diapirs.
- 833 4. Where both salt layers are developed, the topography created by the Zechstein Group
834 halokinesis influences the development of salt-related structures in the overlying
835 Uilleann Halite Member, exemplified in the parallel salt pillow and salt wall pair
836 observed in the Corrib structure. This kinematic interaction may serve as a framework
837 for the structural evolution of similar structures in other basins with multiple
838 stratigraphically discrete layers of salt.
- 839 5. An improved understanding of the distribution and composition of Permian and Triassic
840 salt in the Slyne and Erris basins and in undrilled basins along the Irish Atlantic margin
841 indicates that the framework of sedimentary basins along the Irish Atlantic margin may
842 have been established as early as the Late Permian.

843 References

- 844 Alves, T.M., Moita, C., Sandnes, F., Cunha, T., Monteiro, J.H. & Pinheiro, L.M. 2006.
845 Mesozoic-Cenozoic evolution of North Atlantic continental-slope basins: The Peniche
846 basin, western Iberian margin. *AAPG Bulletin*, **90**, 31–60.
- 847 Ambassador 1962. Dowra No. 1 Well Report. Ambassador Irish Oil Company.
- 848 Amoco 1978. Well 19/5-1 Geological Completion Report. Amoco Ireland Exploration
849 Company, compiled by Odell, R.T. & Thomas, I.W.
- 850 Amoco 1979. Wells 12/13-1 and 12/13-1A Geological Completion Report. Amoco Ireland
851 Exploration Company, compiled by Odell, R.T. & Walker, D.
- 852 Anderson, H., Walsh, J.J. & Cooper, M.R. 2018. The development of a regional-scale
853 intraplate strike-slip fault system; Alpine deformation in the north of Ireland. *Journal of*
854 *Structural Geology*, **116**, 47–63.
- 855 Biancotto, F., Hardy, R.J.J., Jones, S.M., Brennan, D. & White, N.J. 2007. Estimating
856 denudation from seismic velocities offshore NW Ireland. *Society of Exploration*
857 *Geophysicists - 77th SEG International Exposition and Annual Meeting, SEG 2007*,
858 407–411.
- 859 BP 1979. Ireland, Porcupine Basin Well 26/22-1A Geological Completion Report. BP
860 Petroleum Development Ltd. (Irish Branch), compiled by Dryden, G.J.
- 861 Britoil 1986. Eire Licence 1/82 evaluation of well 35/19-1. Britoil plc, compiled by Harvey, M.
862 A. & Wild, J. L.
- 863 Brown, A.R. 2001. Calibrate yourself to your data! A vital first step in seismic interpretation.
864 *Geophysical Prospecting*, **49**, 729–733.
- 865 Chapman, T.J. 1989. The Permian to Cretaceous structural evolution of the Western
866 Approaches Basin (Melville sub-basin), UK. *Geological Society, London, Special*
867 *Publications*, **44**, 177–200.
- 868 Chapman, T.J., Broks, T.M., Corcoran, D.V., Duncan, L.A. & Dancer, P.N. 1999. The
869 structural evolution of the Erris Trough, offshore northwest Ireland, and implications for
870 hydrocarbon generation. *Petroleum Geology of Northwest Europe: Proceedings of the*
871 *5th Conference*, 455–469.
- 872 Chew, D.M. & Stillman, C.J. 2009. Late Caledonian orogeny and magmatism. *In: The*
873 *Geology of Ireland*. 143–173.
- 874 Coleman, A.J., Jackson, C.A.L. & Duffy, O.B. 2017. Balancing sub- and supra-salt strain in
875 salt-influenced rifts: Implications for extension estimates. *Journal of Structural Geology*,
876 **102**, 208–225.
- 877 Colin, J.-P., Ioannides, N.S. & Vining, B. 1992. Mesozoic stratigraphy of the Goban Spur,
878 offshore south-west Ireland. *Marine and Petroleum Geology*, **9**, 527–541.

- 879 Cooper, M.R., Anderson, H., Walsh, J.J., Van Dam, C.L., Young, M.E., Earls, G. & Walker,
880 A. 2012. Palaeogene Alpine tectonics and Icelandic plume-related magmatism and
881 deformation in Northern Ireland. *Journal of the Geological Society*, **169**, 29–36.
- 882 Corcoran, D. V & Doré, A.G. 2002. Depressurization of hydrocarbon-bearing reservoirs in
883 exhumed basin settings: evidence from Atlantic margin and borderland basins.
884 *Exhumation of the North Atlantic Margin: Timing, Mechanisms and Implications for*
885 *Petroleum Exploration*, **196**, 457–483.
- 886 Corcoran, D. V & Mecklenburgh, R. 2005. Exhumation of the Corrib Gas Field, Slyne Basin,
887 offshore Ireland. *Petroleum Geoscience*, **11**, 239–256.
- 888 Corfield, S., Murphy, N. & Parker, S. 1999. The structural and stratigraphic framework of the
889 Irish Rockall Trough. *Geological Society, London, Petroleum Geology Conference*
890 *series*, **5**, 407–420.
- 891 Coward, M.P. 1995. Structural and tectonic setting of the Permo-Triassic basins of northwest
892 Europe. *Geological Society, London, Special Publications*, **91**, 7–39.
- 893 Cunningham, G.A. & Shannon, P.M. 1997. The Erris Ridge: A major geological feature in the
894 NW Irish Offshore Basins. *Journal of the Geological Society*, **154**, 503–508.
- 895 Croker, P.F. and Shannon, P.M. 1987. The evolution and hydrocarbon prospectivity of the
896 Porcupine Basin, Offshore Ireland. *Petroleum Geology of Northwest Europe*, **3**, 633–
897 642.
- 898 Dancer, P.N., Algar, S.T. & Wilson, I.R. 1999. Structural evolution of the Slyne Trough.
899 *Petroleum Geology of Northwest Europe: Proceedings of the 5th Conference on the*
900 *Petroleum Geology of Northwest Europe*, **1**, 445–454.
- 901 Dancer, P.N. & Pillar, N.W. 2001. Exploring in the Slyne Basin: a geophysical challenge. *The*
902 *Petroleum Exploration of Ireland's Offshore Basins*, **188**, 209–222.
- 903 Dancer, P.N., Kenyon-Roberts, S.M., Downey, J.W., Baillie, J.M., Meadows, N.S. & Maguire,
904 K. 2005. The Corrib gas field, offshore west of Ireland. *Geological Society, London,*
905 *Petroleum Geology Conference series*, **6**, 1035–1046.
- 906 Deptuck, M.E. & Kendell, K.L. 2017. A Review of Mesozoic-Cenozoic Salt Tectonics Along
907 the Scotian Margin, Eastern Canada. *In: Permo-Triassic Salt Provinces of Europe,*
908 *North Africa and the Atlantic Margins*. Elsevier, 287–312.
- 909 Doré, A. 1991. The structural foundation and evolution of Mesozoic seaways between
910 Europe and the Arctic. *Palaeogeography, Palaeoclimatology, Palaeoecology*, **87**, 441–
911 492.
- 912 Doré, A.G., Lundin, E.R., Jensen, L.N., Birkeland, O., Eliassen, P.E. & Fichler, C. 1999.
913 Principal tectonic events in the evolution of the northwest European Atlantic margin.
914 *Petroleum Geology of Northwest Europe: Proceedings of the 5th Conference*, 41–61.
- 915 Duffy, O.B., Gawthorpe, R.L., Docherty, M. & Brocklehurst, S.H. 2013. Mobile evaporite
916 controls on the structural style and evolution of rift basins: Danish Central Graben,
917 North Sea. *Basin Research*, **25**, 310–330.

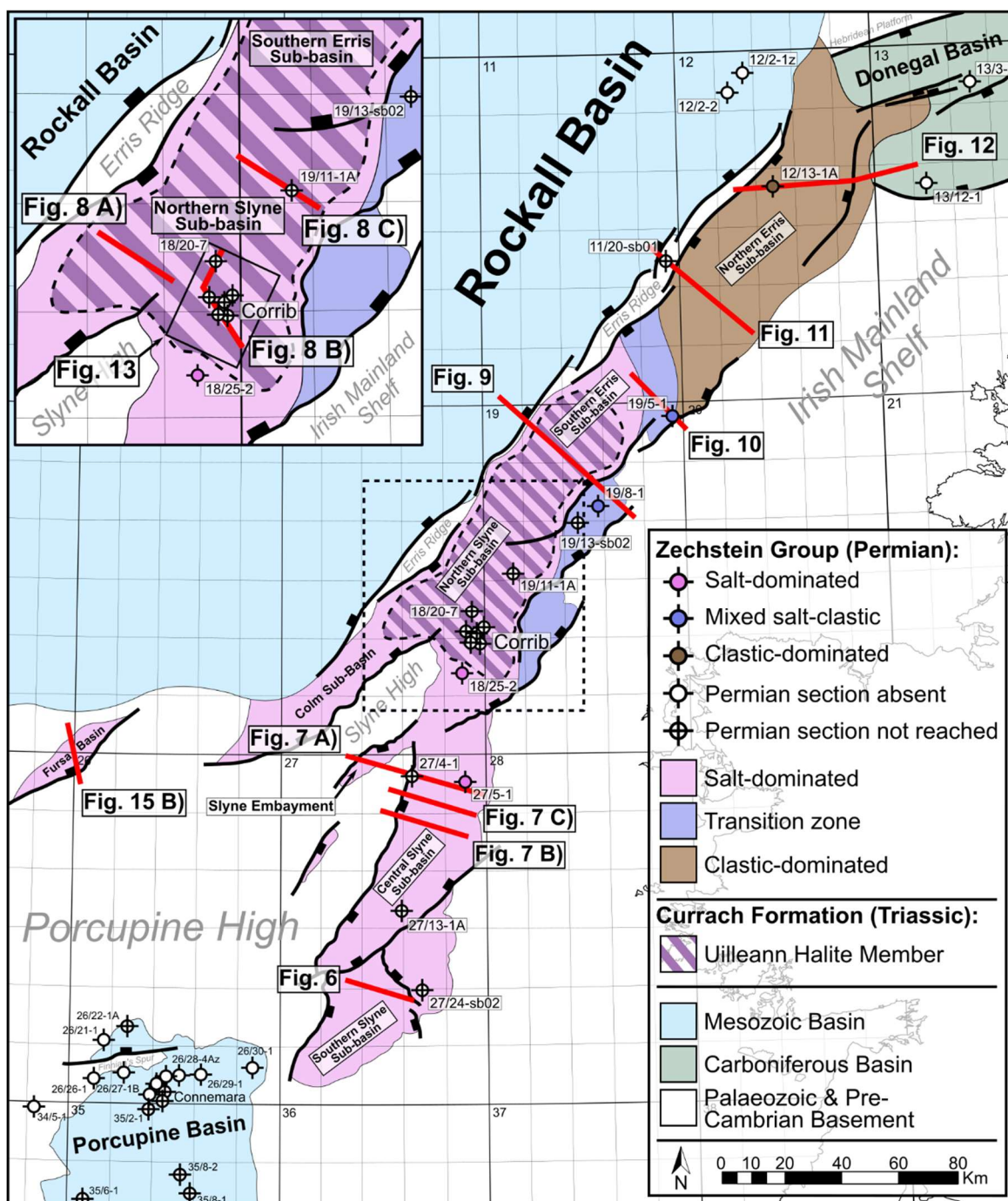
- 918 Dunford, G.M., Dancer, P.N. & Long, K.D. 2001. Hydrocarbon potential of the Kish Bank
919 Basin: integration within a regional model for the Greater Irish Sea Basin. *Geological*
920 *Society, London, Special Publications*, **188**, 135–154.
- 921 Elf 1991. Final Well Report 202/18-1. Elf Enterprise Caledonia Ltd.
- 922 Enterprise 1996. IRE 18/20-1 Geological Completion Report. Enterprise Oil plc, compiled by
923 O'Neill, N., Scotchman, I. & Dancer, N.
- 924 Ferrer, O., Jackson, M.P.A., Roca, E. & Rubinat, M. 2012. Evolution of salt structures during
925 extension and inversion of the Offshore Parentis Basin (Eastern Bay of Biscay).
926 *Geological Society Special Publication*, **363**, 361–380.
- 927 Franklin, J., Tyrrell, S., Morton, A., Frei, D. & Mark, C. 2019. Triassic sand supply to the
928 Slyne Basin, offshore western Ireland – new insights from a multi-proxy provenance
929 approach. *Journal of the Geological Society*, **176**, 1120–1135.
- 930 Fugro. 1994. Field Report Irish Frontier Shallow Coring Project Blocks 19/13 and 27/24 Irish
931 Sector Atlantic Ocean (Volume I).
- 932 Gardiner, P.R.R. & Visscher, H. 1971. Permian–Triassic Transition Sequence at Kingscourt,
933 Ireland. *Nature Physical Science*, **229**, 209–210.
- 934 Gardiner, P.R.R. & McArdle, P. 1992. The geological setting of Permian gypsum and
935 anhydrite deposits in the Kinscourt district, counties Cavan, Meath and Monaghan. *The*
936 *Irish minerals industry, 1980 – 1990*, 301-316
- 937 Gerlings, J., Hopper, J.R., Fyhn, M.B.W. & Frandsen, N. 2017. Mesozoic and older rift
938 basins on the SE Greenland Shelf offshore Ammassalik. *Geological Society Special*
939 *Publication*, **447**, 375–392.
- 940 Glennie, K.W., 1997. History of exploration in the southern North Sea. *Geological Society,*
941 *London, Special Publications*, **123**, 5-16.
- 942 Grennan, E. 1992. The Glangevlin gypsum deposit, Co. Cavan. *The Irish minerals*
943 *industry, 1980 - 1990*, 317-325.
- 944 Hansen, T. H., Clausen, O. R., & Andresen, K. J. (in review) 2020. Thick- and thin-skinned
945 basin inversion in the Danish Central Graben, North Sea – the role of deep evaporites
946 and basement kinematics. *Solid Earth Discuss.* <https://doi.org/10.5194/se-2020-127>
- 947 Houghton, P., Praeg, D., Shannon, P., Harrington, G., Higgs, K., Amy, L., Tyrrell, S. &
948 Morrissey, T. 2005. First results from shallow stratigraphic boreholes on the eastern
949 flank of the Rockall Basin, offshore western Ireland. *Geological Society, London,*
950 *Petroleum Geology Conference series*, **6**, 1077–1094.
- 951 Hitchen, K., Stoker, M.S., Evans, D. & Beddoe-Stephens, B. 1995. Permo-Triassic
952 sedimentary and volcanic rocks in basins to the north and west of Scotland. *Geological*
953 *Society, London, Special Publications*, **91**, 87–102.
- 954 Hudec, M.R. & Jackson, M.P.A. 2007. Terra infirma: Understanding salt tectonics. *Earth-*
955 *Science Reviews*, **82**, 1–28.

- 956 Hutton, D.H.W. & Alsop, G.I. 1996. The Caledonian strike-swing and associated lineaments
957 in NW Ireland and adjacent areas: sedimentation, deformation and igneous intrusion
958 patterns. *Journal of the Geological Society*, **153**, 345–360.
- 959 Illing, L. V & Griffith, A.E. 1986. Gas Prospects in the 'Midland Valley' of Northern Ireland.
960 *Geological Society, London, Special Publications*, **23**, 73–84.
- 961 IS16/04 Technical Report prepared for the Irish Shelf Petroleum Studies Group (ISPSG),
962 2019. *The Standard Stratigraphic Nomenclature of Offshore Ireland: An Integrated*
963 *Lithostratigraphic, Biostratigraphic and Sequence Stratigraphic Framework*, Dublin: Irish
964 Petroleum Infrastructure Programme (PIP).
- 965 Jackson, C.A.L. & Lewis, M.M. 2016. Structural style and evolution of a salt-influenced rift
966 basin margin; the impact of variations in salt composition and the role of polyphase
967 extension. *Basin Research*, **28**, 81–102.
- 968 Jackson, C.A.-L. & Stewart, S.A. 2017. Composition, Tectonics, and Hydrocarbon
969 Significance of Zechstein Supergroup Salt on the United Kingdom and Norwegian
970 Continental Shelves. In: *Permo-Triassic Salt Provinces of Europe, North Africa and the*
971 *Atlantic Margins*. Elsevier, 175–201.
- 972 Jackson, C.A.L., Elliott, G.M., Royce-Rogers, E., Gawthorpe, R.L. & Aas, T.E. 2019. Salt
973 thickness and composition influence rift structural style, northern North Sea, offshore
974 Norway. *Basin Research*, **31**, 514–538.
- 975 Jackson, D.I. & Mulholland, P. 1993. Tectonic and stratigraphic aspects of the East Irish Sea
976 Basin and adjacent areas: contrasts in their post-Carboniferous structural styles.
977 *Geological Society, London, Petroleum Geology Conference series*, **4**, 791–808.
- 978 Jackson, M.P.A. & Vendeville, B.C. 1994. Regional extension as a geologic trigger for
979 diapirism. *Geological Society of America Bulletin*, **106**, 57–73.
- 980 Jackson, M.P., & Hudec, M.R. 2017. *Salt tectonics: Principles and practice*. Cambridge
981 University Press.
- 982 Jansa, L.F., Bujak, J.P. & Williams, G.L. 1980. Upper Triassic salt deposits of the western
983 North Atlantic. *Canadian Journal of Earth Sciences*, **17**, 547–559.
- 984 Jolley, D.W. & Bell, B.R. 2002. The evolution of the North Atlantic Igneous Province and the
985 opening of the NE Atlantic rift. *Geological Society, London, Special Publications*, **197**,
986 1–13.
- 987 Knott, S.D., Burchell, M.T., Jolley, E.J. & Fraser, A.J. 1993. Mesozoic to Cenozoic plate
988 reconstructions of the North Atlantic and hydrocarbon plays of the Atlantic margins.
989 *Petroleum Geology of Northwest Europe: Proceedings of the 4th Conference*, 953–974.
- 990 Le Breton, E., Cobbold, P.R. & Zanella, A. 2013. Cenozoic reactivation of the Great Glen
991 Fault, Scotland: additional evidence and possible causes. *Journal of the Geological*
992 *Society*, **170**, 403–415.
- 993 Lundin 2006. Well 13/12-1 Inishbeg Prospect End of Well Report. Lundin Britain Ltd.,
994 compiled by Craig, D. & Welding, P.

- 995 McCann, N. 1988. An Assessment of the Subsurface Geology between Magilligan Point and
996 Fair Head, Northern Ireland. *Irish Journal of Earth Sciences*, **9**, 71–78.
- 997 McKie, T. & Shannon, P.M. 2011. Comment on ‘The Permian-Triassic transition and the
998 onset of Mesozoic sedimentation at the northwestern peri Tethyan domain scale:
999 Palaeogeographic maps and geodynamic implications’ by S. Bourquin, A. Bercovici, J.
1000 López-Gomez, J. B. Diez, J. Broutin, A. . *Palaeogeography, Palaeoclimatology,*
1001 *Palaeoecology*, **311**, 136–143.
- 1002 McKie, T. 2017. Paleogeographic Evolution of Latest Permian and Triassic Salt Basins in
1003 Northwest Europe. *In: Permo-Triassic Salt Provinces of Europe, North Africa and the*
1004 *Atlantic Margins*. Elsevier, 159–173.
- 1005 Naylor, D. & Shannon, P., 1982. Geology of offshore Ireland and west Britain.
- 1006 Naylor, D. 1992. The post-Variscan history of Ireland. *Geological Society, London, Special*
1007 *Publications*, **62**, 255–275, <https://doi.org/10.1144/GSL.SP.1992.062.01.21>.
- 1008 Naylor, D., Haughey, N., Clayton, G. & Graham, J.R. 1993. The Kish Bank Basin, offshore
1009 Ireland. *Petroleum Geology of Northwest Europe: Proceedings of the 4th Conference*,
1010 **4**, 845–855, <https://doi.org/10.1144/0040845>.
- 1011 Pena dos Reis, R., Pimentel, N., Fainstein, R., Reis, M. & Rasmussen, B. 2017. Influence of
1012 Salt Diapirism on the Basin Architecture and Hydrocarbon Prospects of the Western
1013 Iberian Margin. *In: Permo-Triassic Salt Provinces of Europe, North Africa and the*
1014 *Atlantic Margins*. Elsevier, 313–329.
- 1015 Petroleum Affairs Division. 2005. *Petroleum Systems Analysis of the Slyne, Erris and*
1016 *Donegal Basins Offshore Ireland - Digital Atlas*. PAD, Special Publications, Dublin,
1017 **1/05**.
- 1018 Quinn, M.F., Smith, K. & Bulat, J. 2010. A Geological Interpretation of the Nearshore Area
1019 between Belfast Lough and Cushendun, Northern Ireland, Utilising a Newly Acquired
1020 2D Seismic Dataset to Explore for Salt Layers for Possible Gas Storage within Man-
1021 Made Caverns. *British Geological Survey Commissioned Report CR/10/069*.
- 1022 Raine, R., Copestake, P., Simms, M.J. & Boomer, I. 2020. Uppermost Triassic to Lower
1023 Jurassic sediments of the island of Ireland and its surrounding basins. *Proceedings of*
1024 *the Geologists’ Association*.
- 1025 Ramos, A., Fernández, O., Muñoz, J.A. & Terrinha, P. 2017. Impact of basin structure and
1026 evaporite distribution on salt tectonics in the Algarve Basin, Southwest Iberian margin.
1027 *Marine and Petroleum Geology*, **88**, 961–984.
- 1028 Robinson, K.W., Shannon, P.M. and Young, D.G.G. 1981. The Fastnet Basin: An Integrated
1029 Analysis. *In: Illing, L. V. and Hobson, G. D. (eds) Petroleum Geology of the Continental*
1030 *Shelf of North-West Europe*.
- 1031 Rojo, L.A., Cardozo, N., Escalona, A. & Koyi, H. 2019. Structural style and evolution of the
1032 Nordkapp Basin, Norwegian Barents Sea. *AAPG Bulletin*, **103**, 2177–2217.
- 1033 Schiffer, C., Doré, A.G., Foulger, G.R., Franke, D., Geoffroy, L., Gernigon, L., Holdsworth,
1034 R.E., Kusznir, N., Lundin, E., McCaffrey, K., Peace, A.L., Petersen, K.D., Phillips, T.B.,

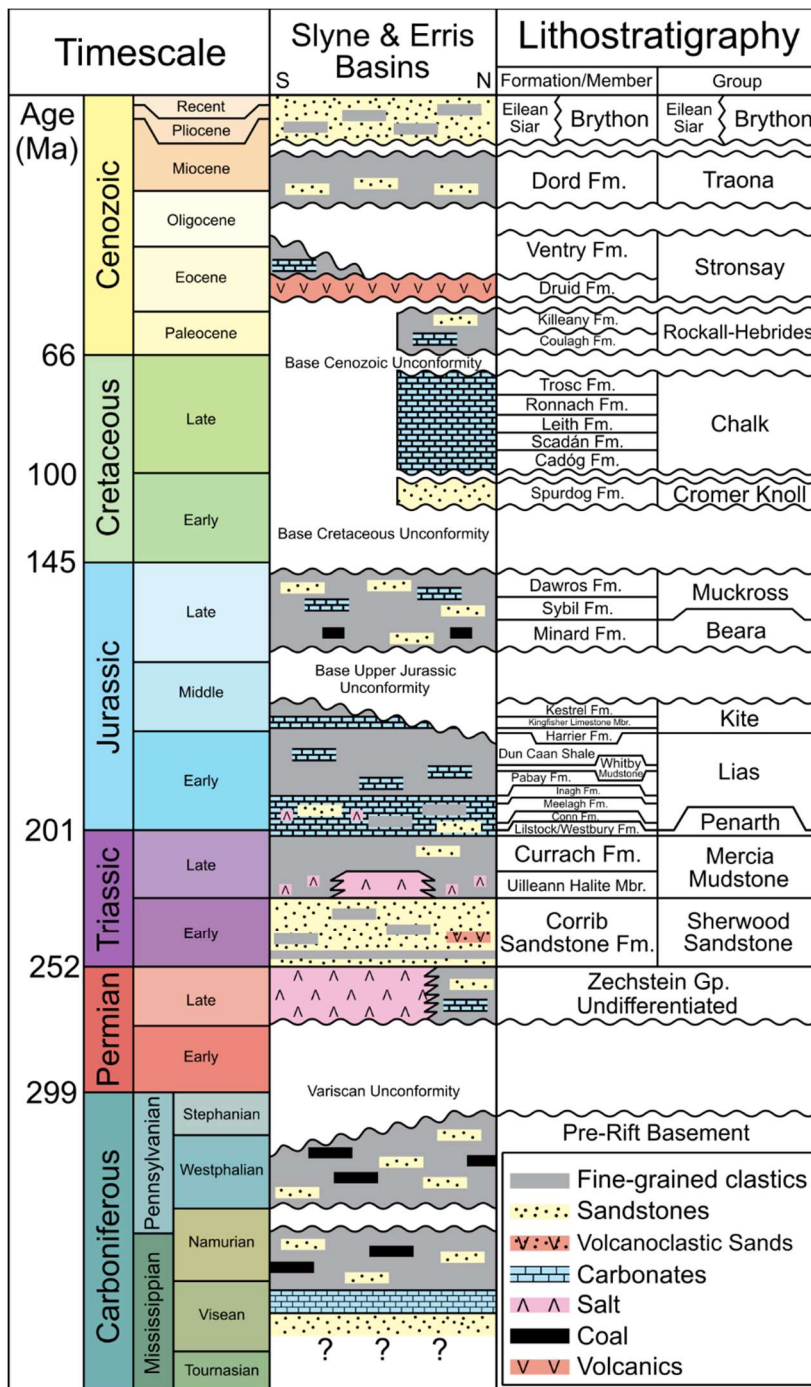
- 1035 Stephenson, R., Stoker, M.S. & Welford J.K. 2019. Structural inheritance in the North
1036 Atlantic. *Earth-Science Reviews*, 102975.
- 1037 Scotese, C.R. & Schettino, A. 2017. Late Permian-Early Jurassic Paleogeography of
1038 Western Tethys and the World. *In: Permo-Triassic Salt Provinces of Europe, North*
1039 *Africa and the Atlantic Margins*. Elsevier, 57–95.
- 1040 Shannon, P.M. 1991. Tectonic framework and petroleum potential of the Celtic Sea, Ireland.
1041 *First Break*, **9**, <https://doi.org/10.3997/1365-2397.1991006>.
- 1042 Shannon, P.M. & Naylor, D. 1998. An assessment of Irish offshore basins and petroleum
1043 plays. *Journal of Petroleum Geology*, **21**, 125–152.
- 1044 Shell 2009. IRE 12/2-1 West Dooish Exploration Well End of Well Report – Volume 2
1045 Subsurface Section. Shell E&P Ireland Ltd.
- 1046 StatoilHydro 2009. Well 19/8-1 Cashel Prospect End of Well Report. Statoil Exploration
1047 (Ireland) Ltd., compiled by MacTiernan, B., Kleppa, S., Hunnes, O., Sigve-Selnes, K. &
1048 Igbineweka, O.J.
- 1049 Stewart, S.A., Harvey, M.J., Otto, S.C. & Weston, P.J. 1996. Influence of salt on fault
1050 geometry: examples from the UK salt basins. *Geological Society, London, Special*
1051 *Publications*, **100**, 175–202.
- 1052 Stewart, S.A. 2007. Salt tectonics in the North Sea Basin: a structural style template for
1053 seismic interpreters. *Geological Society, London, Special Publications*, **272**, 361–396.
- 1054 Stoker, M.S., Stewart, M.A., Shannon, P.M., Bjerager, M., Nielsen, T., Blischke, A.,
1055 Hjelstuen, B.O., Gaina, C., McDermott, K. & Ólavsdóttir, J. 2017. An overview of the
1056 Upper Palaeozoic–Mesozoic stratigraphy of the NE Atlantic region. *Geological Society,*
1057 *London, Special Publications*, **447**, 11–68, <https://doi.org/10.1144/SP447.2>.
- 1058 Štolfova, K. & Shannon, P.M. 2009. Permo-Triassic development from Ireland to Norway:
1059 basin architecture and regional controls. *Geological Journal*, **44**, 652–676.
- 1060 Steel, R.J. & Wilson, A.C. 1975. Sedimentation and tectonism (?Permo-Triassic) on the
1061 margin of the North Minch Basin. *Journal of the Geological Society*, **131**, 183–200.
- 1062 Swiecicki, T., Wilcockson, P., Canham, A., Whelan, G. & Homann, H. 1995. Dating,
1063 correlation and stratigraphy of the Triassic sediments in the West Shetlands area.
1064 *Geological Society Special Publication*, **91**, 57–85.
- 1065 Tate, M.P. & Dobson, M.R. 1989. Late Permian to early Mesozoic rifting and sedimentation
1066 offshore NW Ireland. *Marine and Petroleum Geology*, **6**, 49–59.
- 1067 Texaco 1978. Well 13/3-1 Final Geological Report. Texaco Ireland Ltd., compiled by Stuart,
1068 I.A.
- 1069 Thomson, A. & McWilliam, A. 2001. The structural style and evolution of the Bróna Basin.
1070 *Geological Society, London, Special Publications*, **188**, 401–410.

- 1071 Trueblood, S. and Morton, N. 1991. Comparative Sequence Stratigraphy and Structural
1072 Styles of the Slyne Trough and Hebrides Basin. *Journal of the Geological Society*, **148**,
1073 197–201, <https://doi.org/10.1144/gsjgs.148.1.0197>.
- 1074 Trueblood, S. 1992. Petroleum geology of the Slyne Trough and adjacent basins. *Geological*
1075 *Society Special Publication*, 315–326.
- 1076 Tyrrell, S., Haughton, P.D.W. & Daly, J.S. 2007. Drainage reorganization during breakup of
1077 Pangea revealed by in-situ Pb isotopic analysis of detrital K-feldspar. *Geology*, **35**,
1078 971–974.
- 1079 Tyrrell, S., Souders, A.K., Haughton, P.D.W., Daly, J.S. & Shannon, P.M. 2010.
1080 Sedimentology, sandstone provenance and palaeodrainage on the eastern Rockall
1081 Basin margin: evidence from the Pb isotopic composition of detrital K-feldspar.
1082 *Geological Society, London, Petroleum Geology Conference series*, **7**, 937–952.
- 1083 Van Hoorn, B. 1987. The south Celtic Sea/Bristol Channel Basin: origin, deformation and
1084 inversion history. *Tectonophysics*, **137**, [https://doi.org/10.1016/0040-1951\(87\)90325-8](https://doi.org/10.1016/0040-1951(87)90325-8).
- 1085 Walsh, A., Knag, G., Morris, M., Quinquis, H., Tricker, P., Bird, C. & Bower, S. 1999.
1086 Petroleum geology of the Irish Rockall Trough – a frontier challenge. *Petroleum*
1087 *Geology of Northwest Europe: Proceedings of the 5th Conference*, 433–444.
- 1088 Withjack, M.O. & Callaway, S. 2000. Active normal faulting beneath a salt layer: An
1089 experimental study of deformation patterns in the cover sequence. *AAPG Bulletin*, **84**,
1090 627–651.
- 1091 Zamora, G., Fleming, M. & Gallastegui, J. 2017. Salt Tectonics Within the Offshore Asturian
1092 Basin. In: *Permo-Triassic Salt Provinces of Europe, North Africa and the Atlantic*
1093 *Margins*. Elsevier, 353–368.



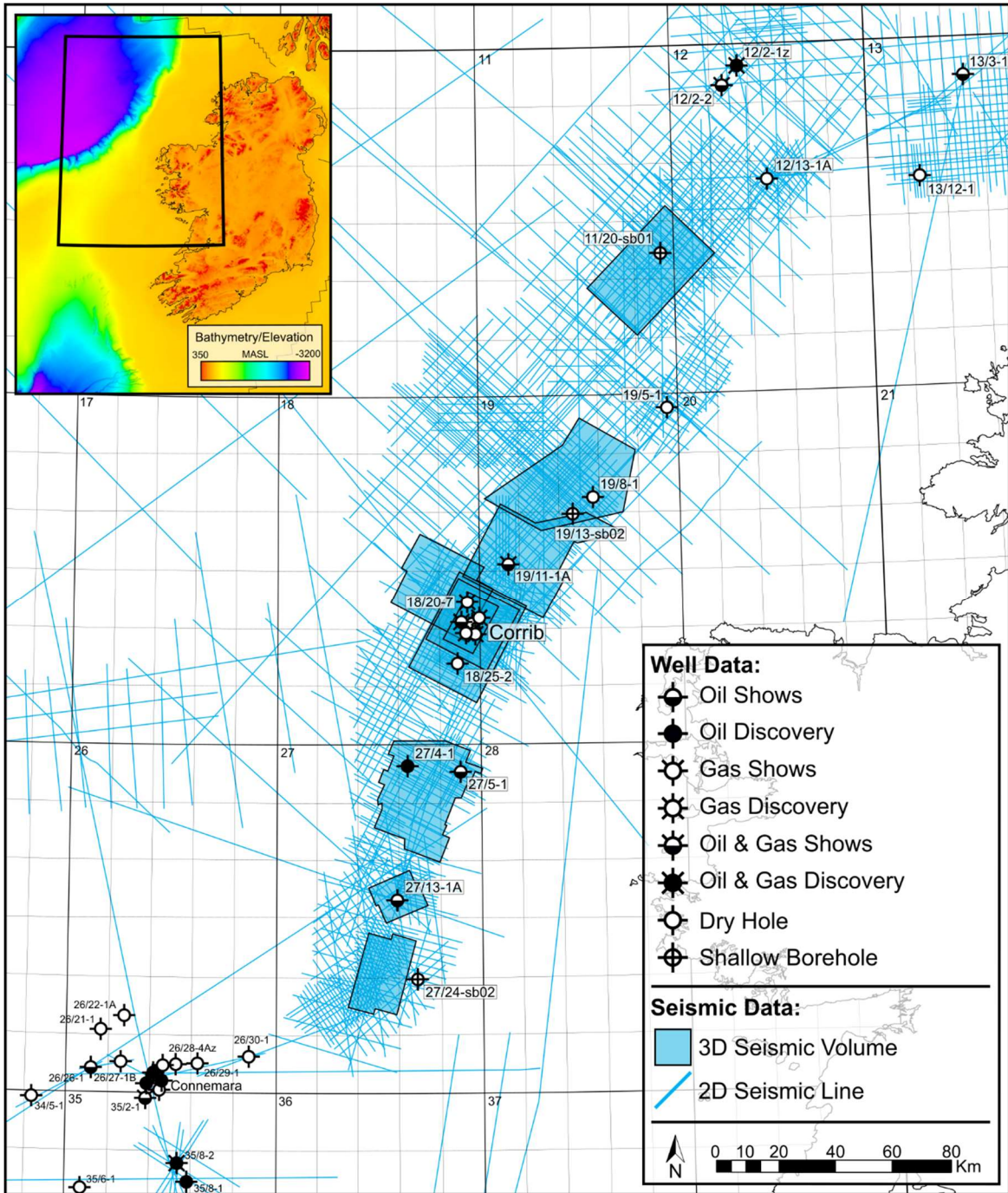
1095

1096 **Figure 1:** Map showing the distribution of Permian and Triassic salt throughout the Slyne and
 1097 Erris basins and neighbouring basins. **Inset Map:** Map showing distribution of salt in the
 1098 Northern Slyne Sub-basin.



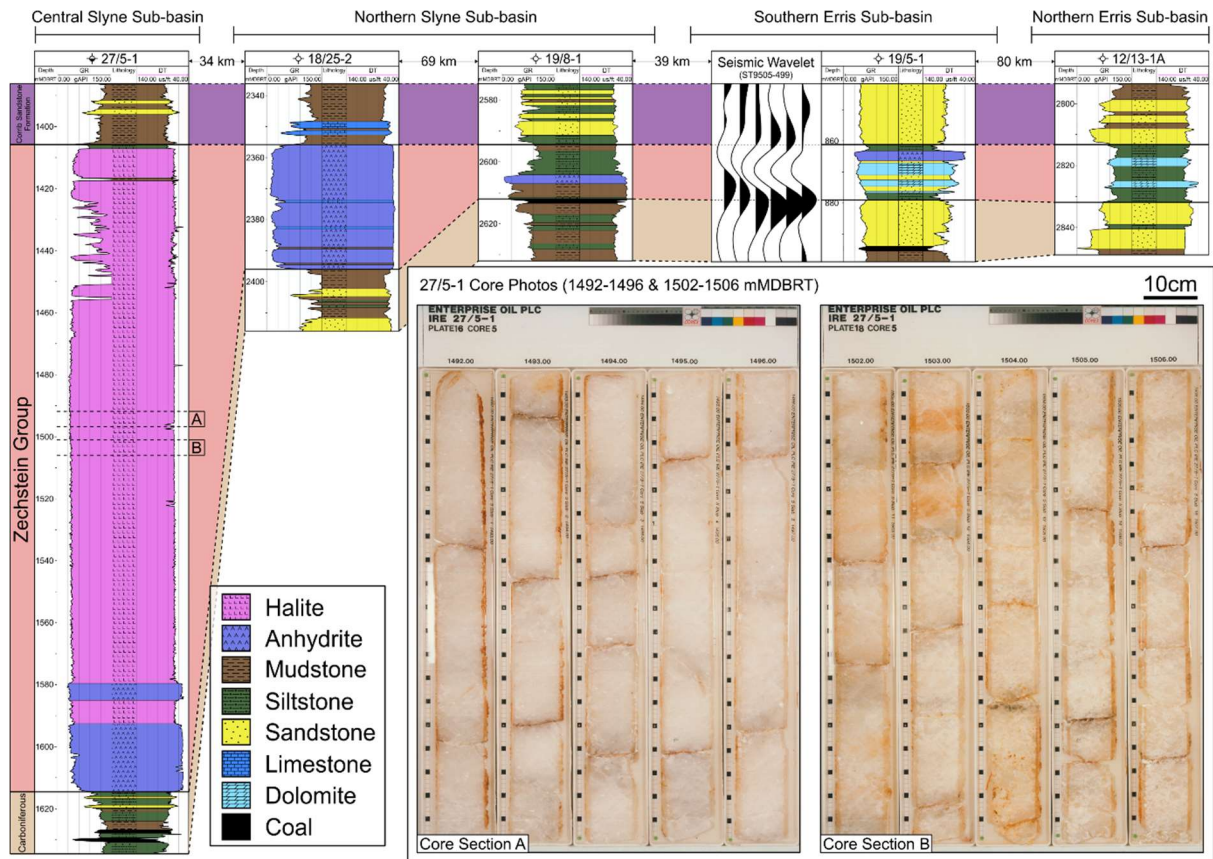
1099

1100 **Figure 2:** Simplified chronostratigraphic chart for the Slyne and Erris basins. Lithostratigraphic
 1101 nomenclature adapted from IS16/04 Technical Report (2019).



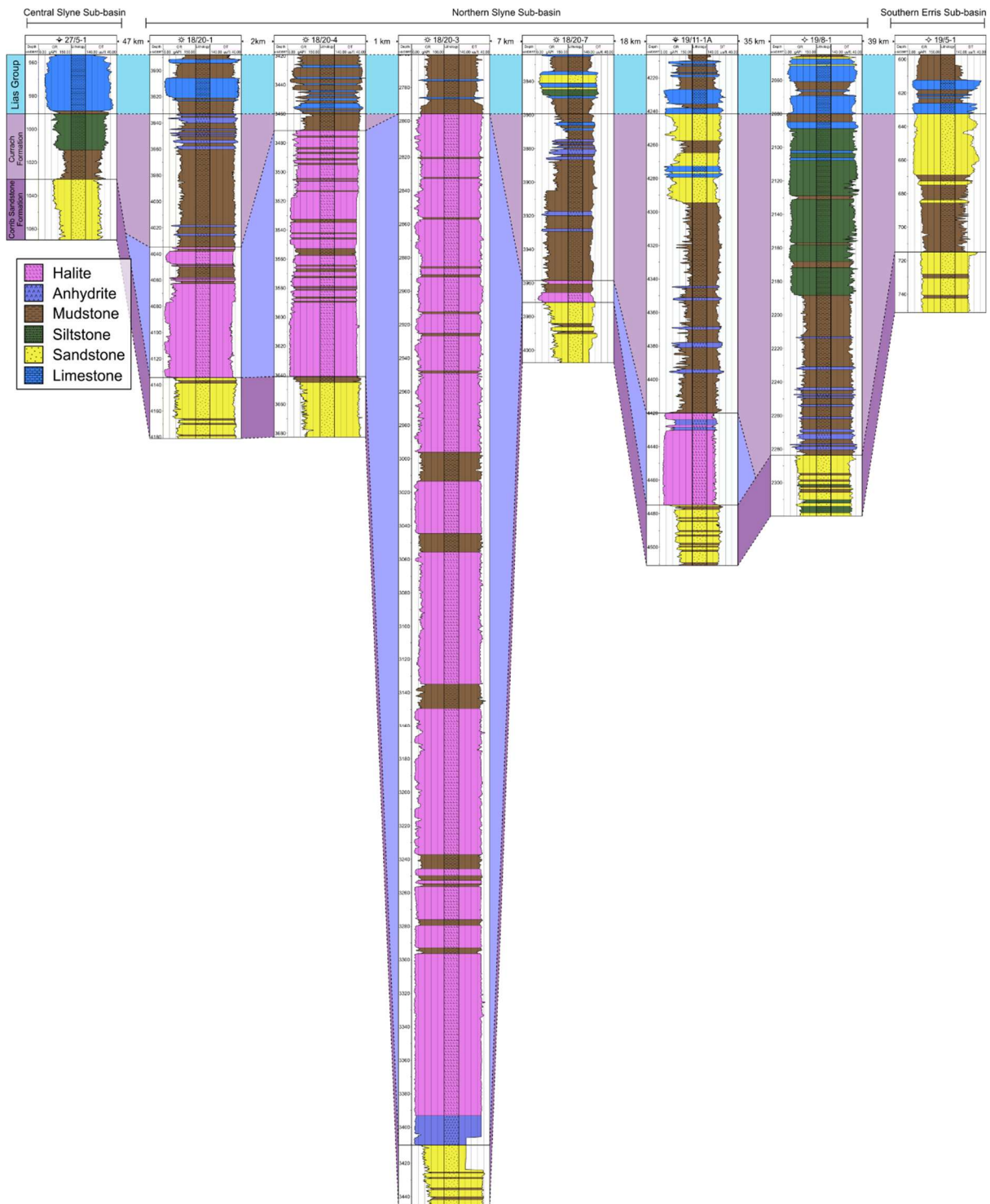
1102

1103 **Figure 3:** Map showing study area and datasets used. ***Inset Map:*** Bathymetry of the study
 1104 *area.*



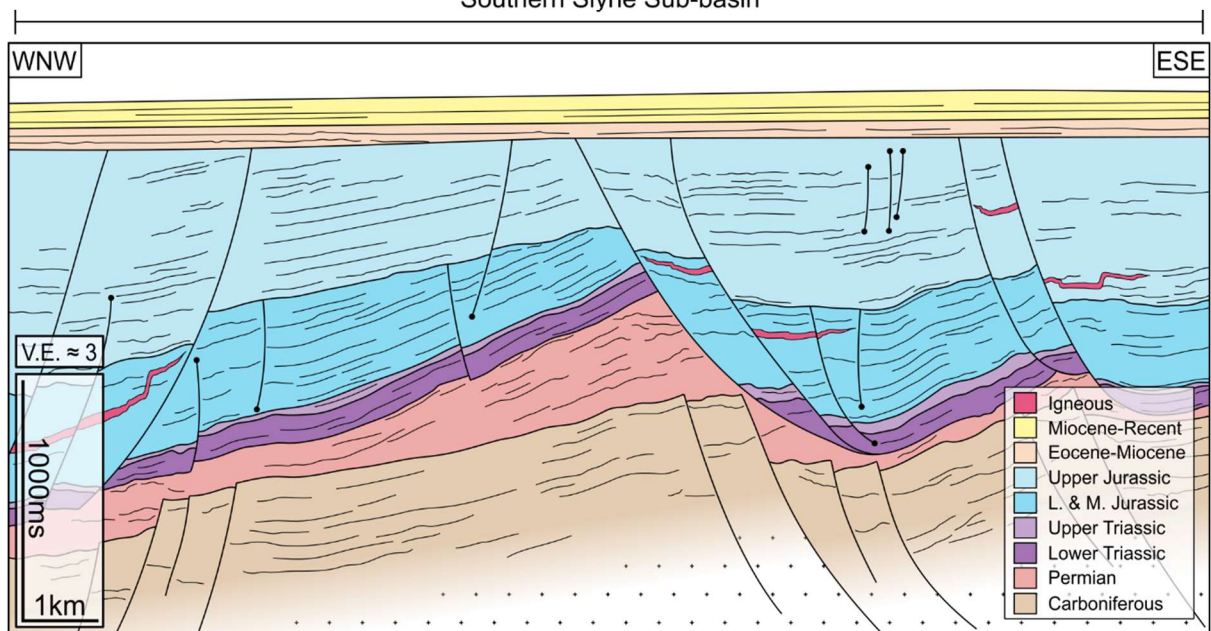
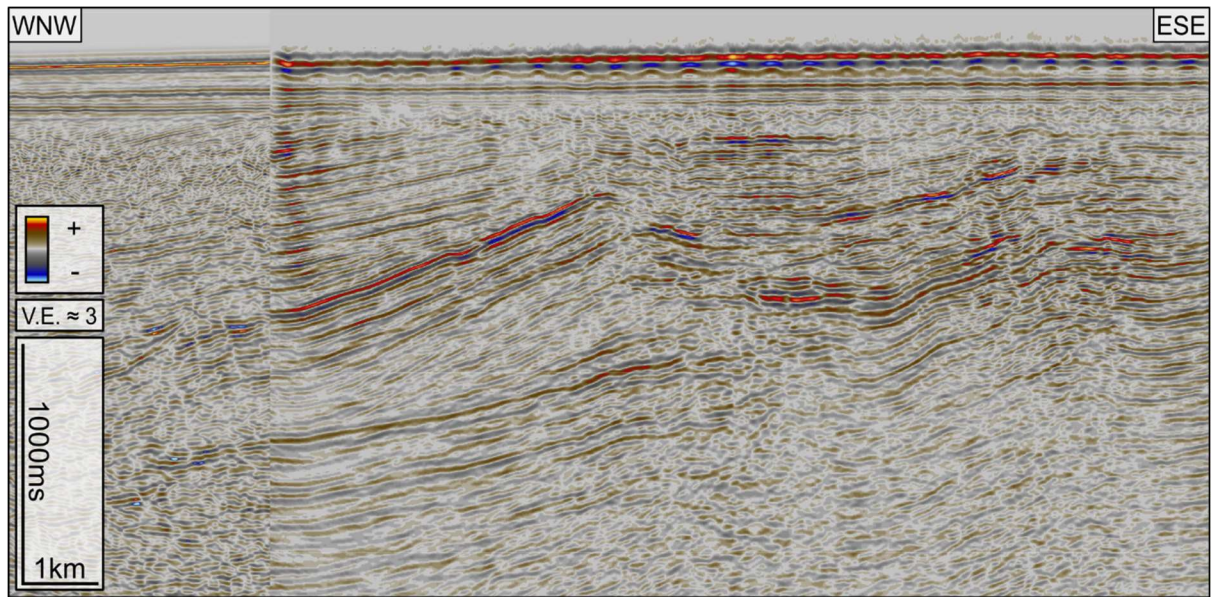
1105

1106 **Figure 4:** Lithological well correlation of the Zechstein Group through the Slyne and Erris
 1107 basins. Correlation is flattened to the top of the Zechstein Group. **Inset:** Select core photos
 1108 from the 27/5-1 well in the central Slyne Basin, showing the massive, crystalline, halite-prone
 1109 Zechstein Group.



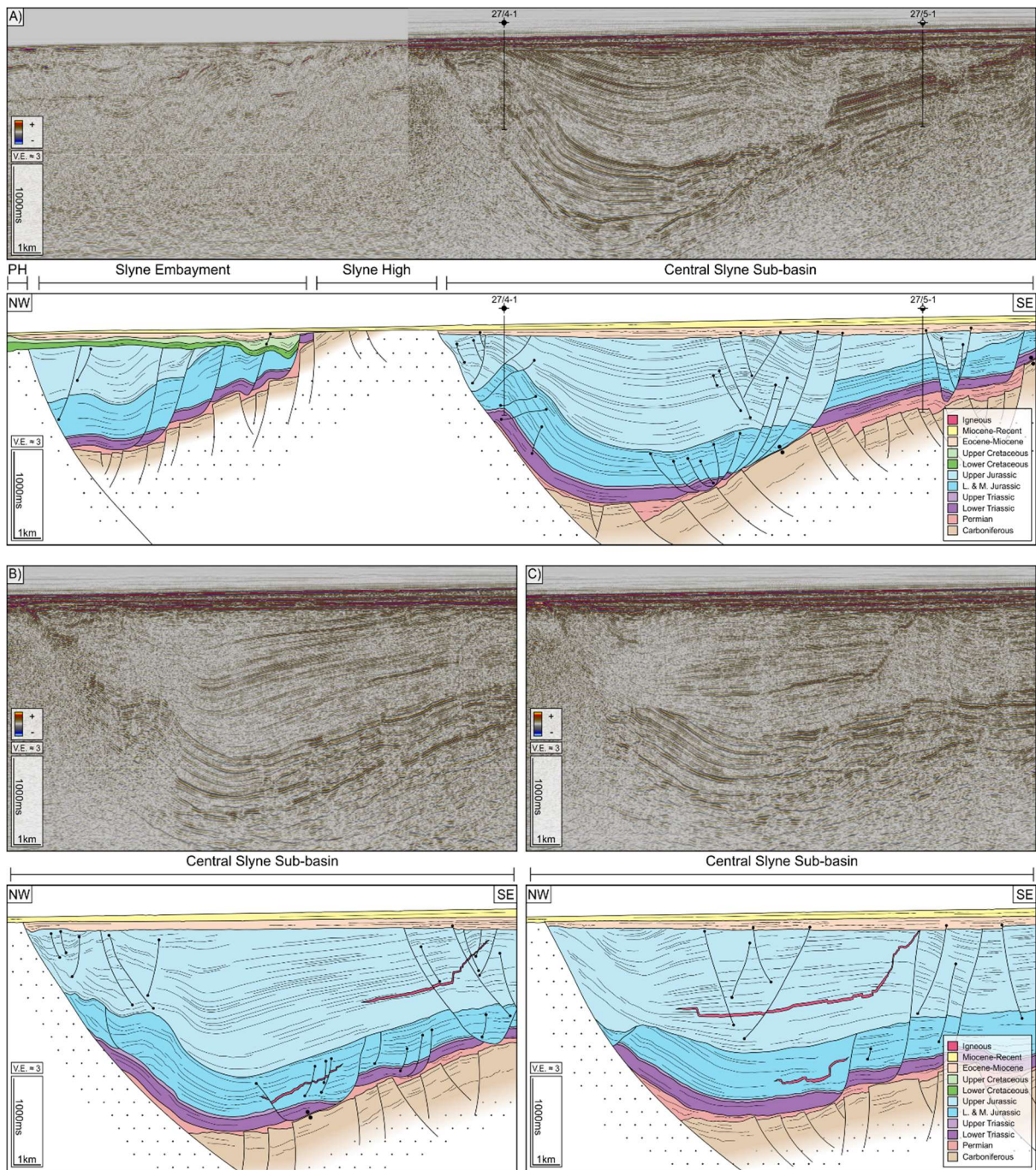
1110

1111 **Figure 5:** Lithological correlation of the Currach Formation and Uilleann Halite Member of
 1112 select wells through the Slyne and Erris basins. Correlation is flattened to the top of the
 1113 Currach Formation.



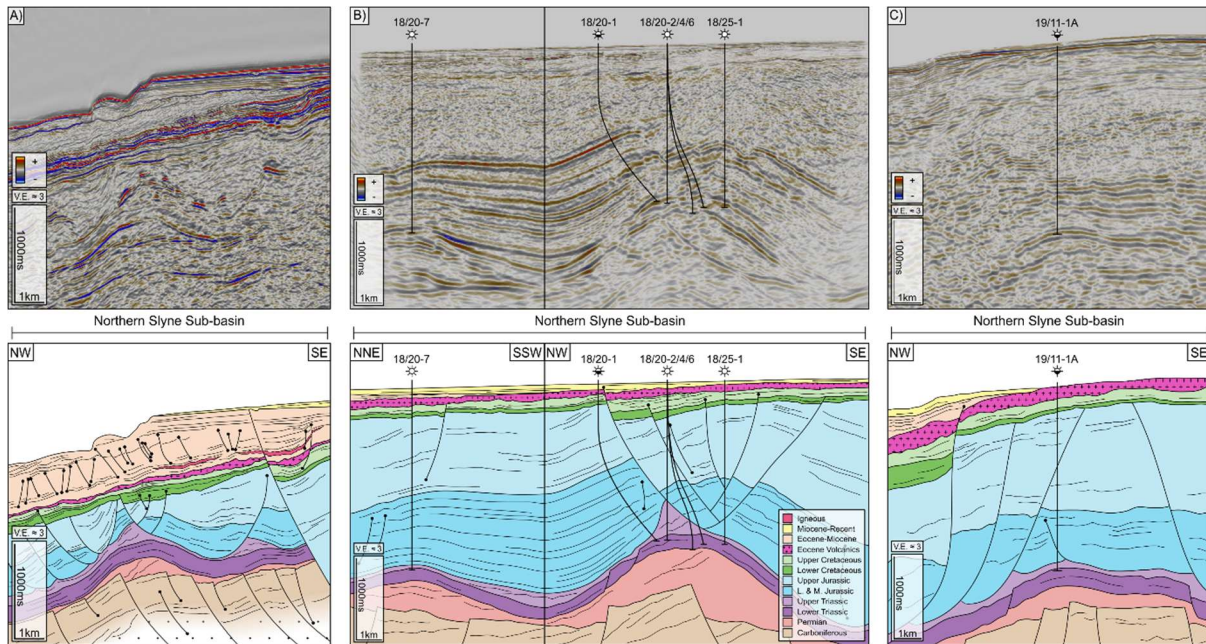
1114

1115 **Figure 6:** Composite seismic section of 2D seismic line TK25-95-32 and crossline 3163 from
 1116 the 2010/01 (SL103D) 3D seismic volume, with accompanying geoseismic interpretation. The
 1117 Middle and Lower Jurassic section is severely eroded on the crest of the fault block cored by
 1118 the large salt roller, with a thicker section preserved in the hanging-wall. See figure 1 for
 1119 seismic line location.



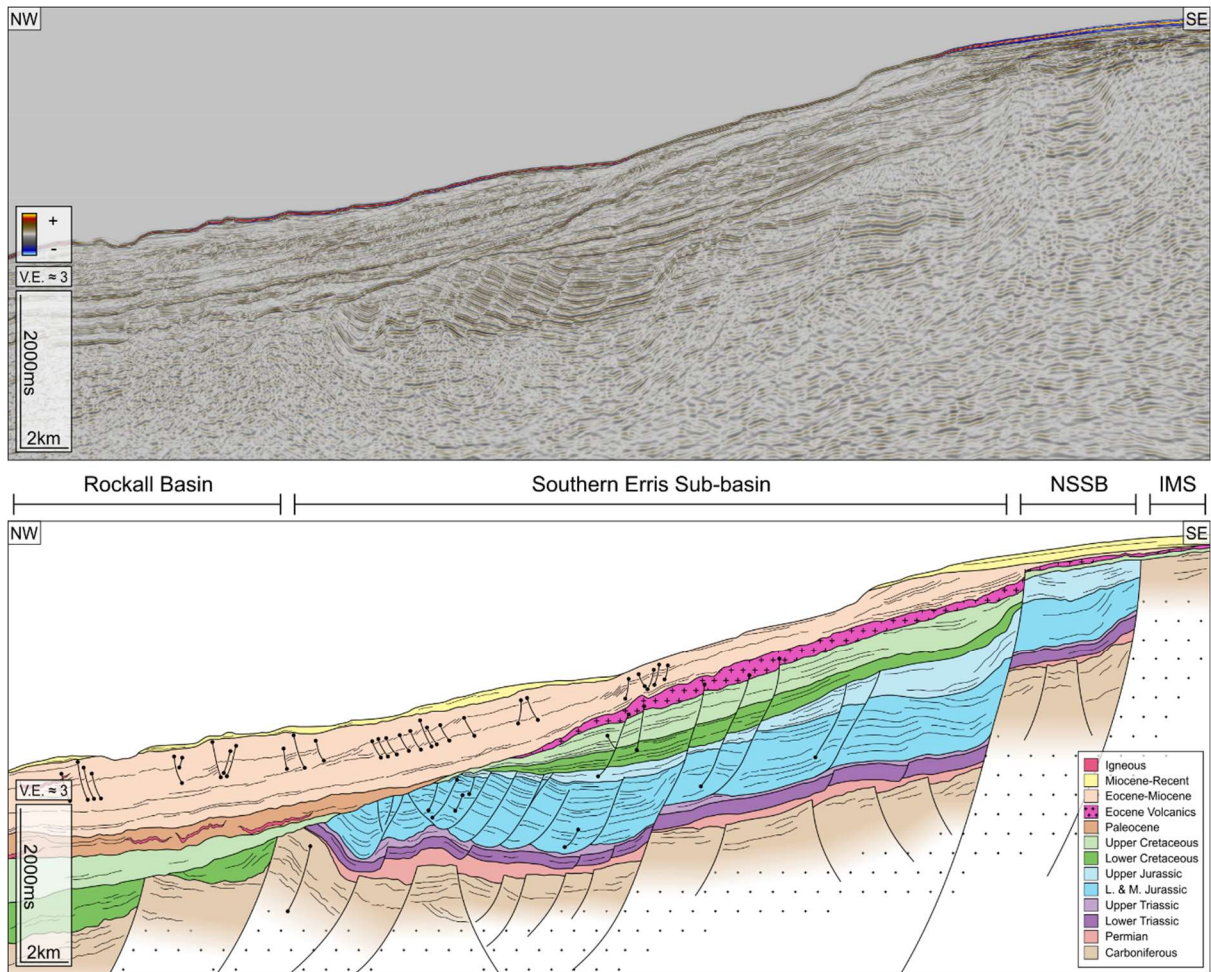
1120

1121 **Figure 7:** Seismic sections from the central Slyne Basin. See figure 1 for seismic line
 1122 locations. **A)** Composite seismic section of 2D seismic line E96IE09-28 and inline 2740 from
 1123 the 2000/08 (E00IE09) 3D seismic volume with accompanying seismic interpretation.
 1124 **Abbreviations:** PH – Porcupine High **B)** Inline 1790 from the 2000/08 (E00IE09) 3D seismic
 1125 volume with accompanying seismic interpretation. **C)** Inline 2040 from the 2000/08 (E00IE09)
 1126 3D seismic volume with accompanying seismic interpretation.



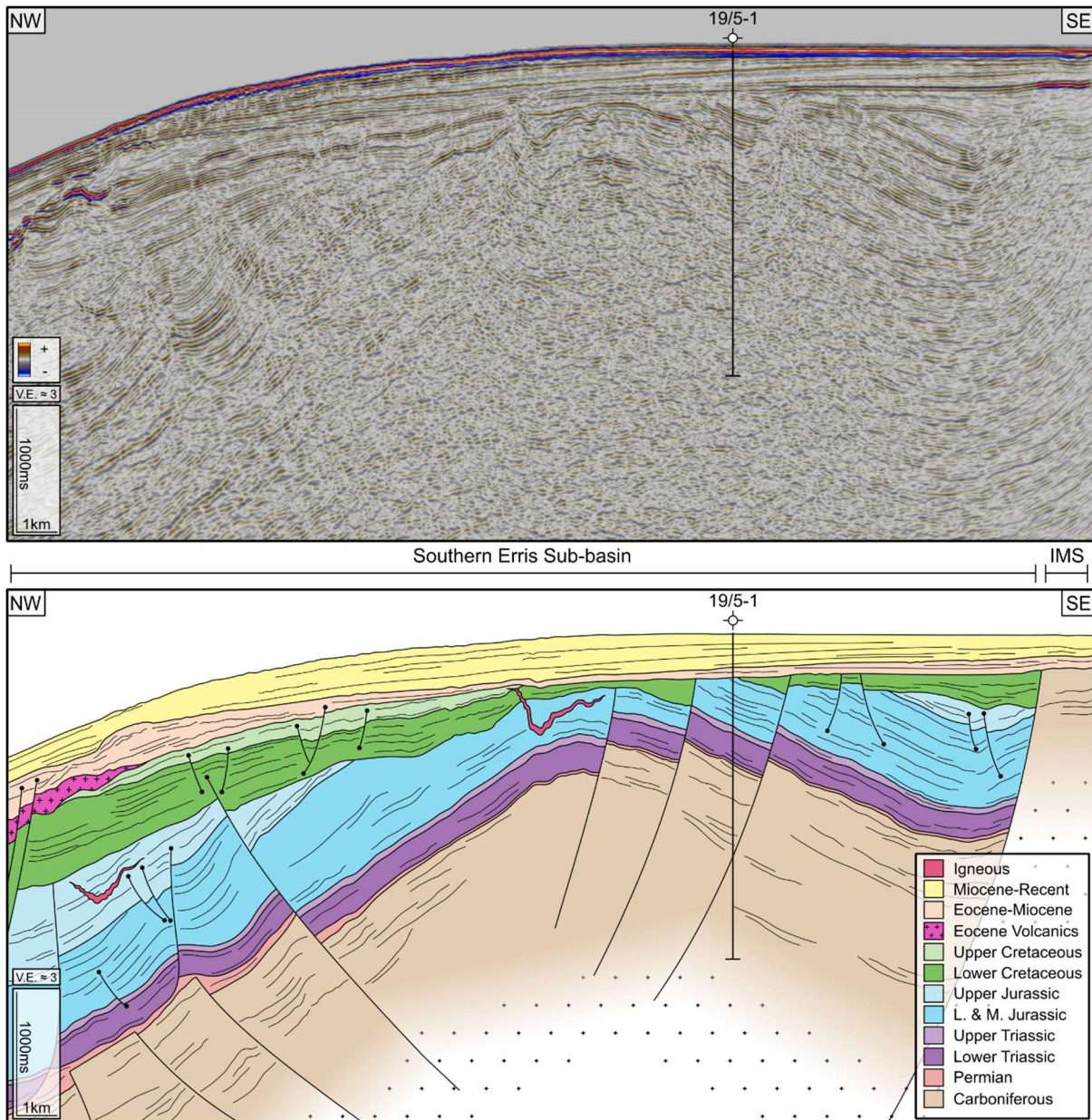
1127

1128 **Figure 8:** Seismic sections from the northern Slyne Basin. See figure 1 for seismic line
 1129 locations. **A)** Inline 1600 from the 2018 Inishkea Reprocessed 3D seismic volume and
 1130 accompanying geoseismic section. A Zechstein Group salt pillow folds the Corrib Sandstone
 1131 Formation, with delamination faults soling out in the Uilleann Halite Member of the Currach
 1132 Formation above the crest of the fold. **B)** Arbitrary line from the 2013-01 (13SH3D) 3D seismic
 1133 volume and accompanying geoseismic interpretation. Two salt-cored folds are visible, one
 1134 containing the 18/20-7 ‘Corrib North’ gas discovery, and the other containing the Corrib Gas
 1135 Field. A major eastward-dipping delamination fold is developed in the Jurassic section above
 1136 the crest of the Corrib structure, soling out above a small salt diapir within the Uilleann Halite
 1137 Member, with a faulted rollover formed in the hanging-wall of this fault. **C)** Arbitrary line from
 1138 the 2001/01 3D seismic volume and accompanying geoseismic section. The salt-cored fold
 1139 tested by the 19/11-1A well is shown, with minor delamination faults forming above, soling out
 1140 in the Uilleann Halite Member. The steep westward dip along the western edge of the structure
 1141 demonstrates the influence of post-rift thermal subsidence in the Rockall Basin.



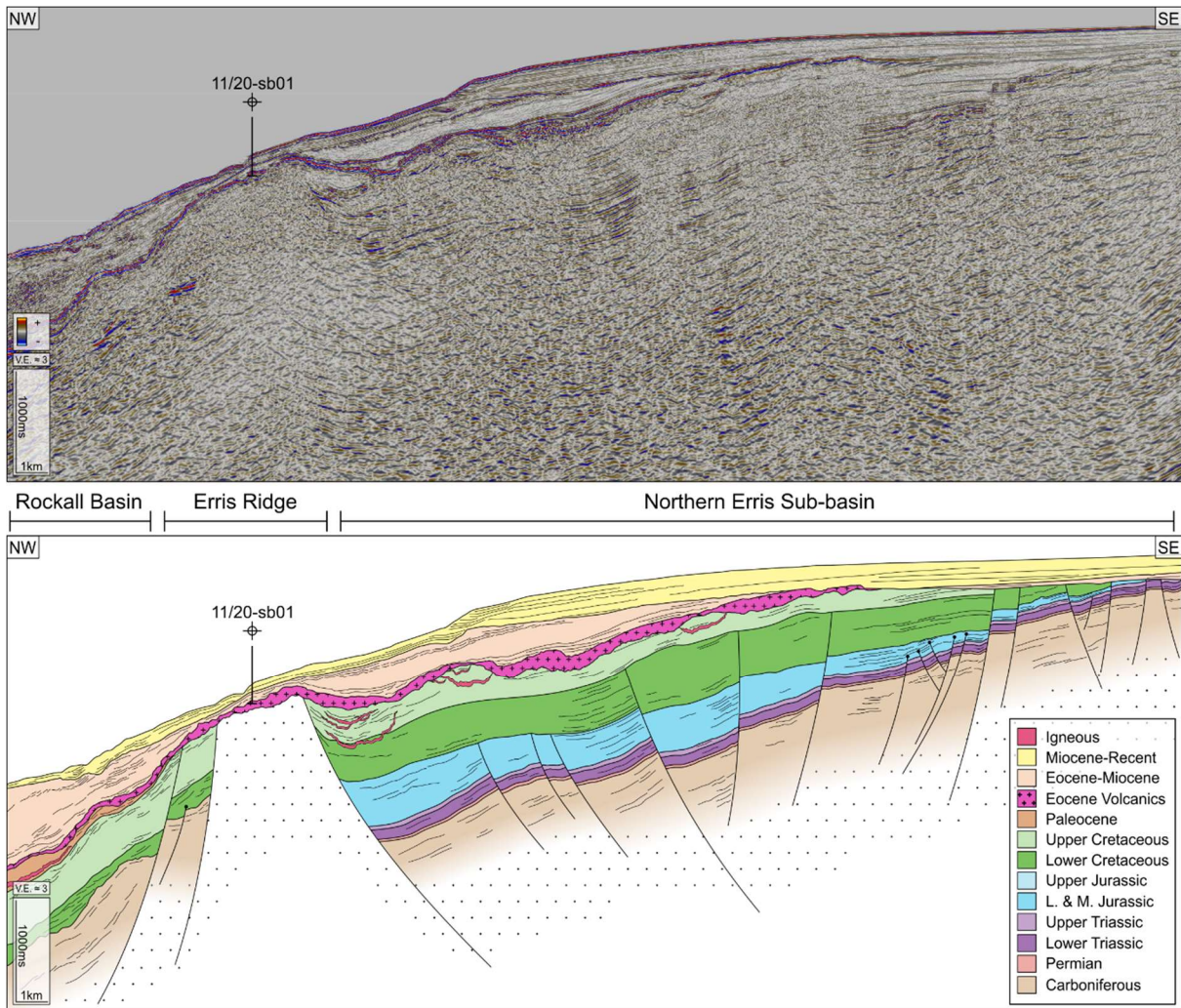
1142

1143 **Figure 9:** 2D seismic line ERM07-6000 and accompanying geoseismic section. The Jurassic
 1144 section in the southern Erris Basin is dominated by tightly spaced, westward-dipping listric
 1145 faults which detach on the Uilleann Halite Member. There is also a Zechstein salt pillow
 1146 evident near the western margin of the basin. Stratigraphy in the Rockall Basin is constrained
 1147 through correlation with the 12/2-1 and 12/2-2 wells to the NE. See figure 1 for seismic line
 1148 location. **Abbreviations:** IMS – Irish Mainland Shelf; NSSB – Northern Slyne Sub-basin.



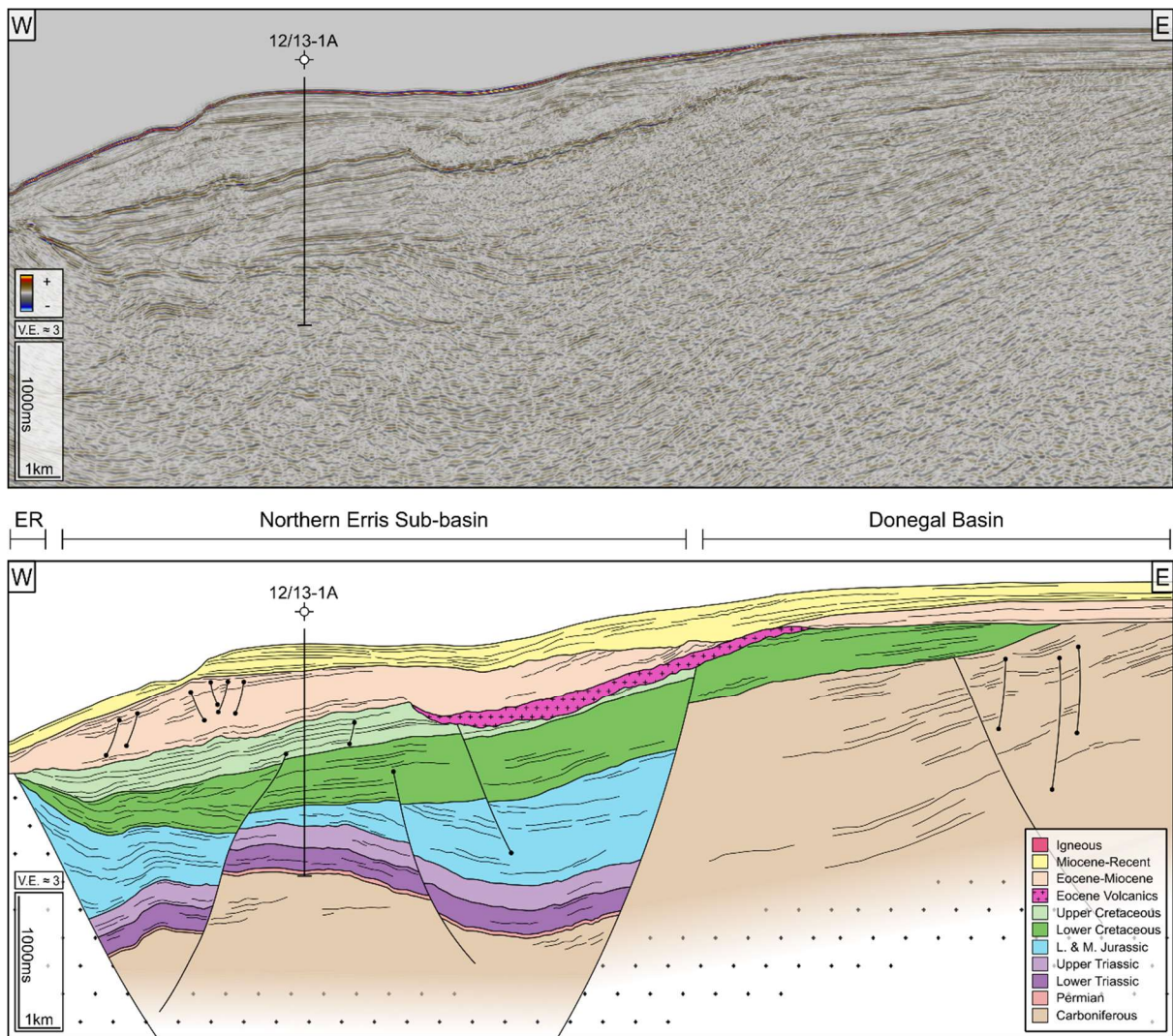
1149

1150 **Figure 10:** 2D seismic line ST9505-449 and accompanying geoseismic section. The
 1151 proportion of salt in the Zechstein Group increase north-westwards. Faults on the eastern side
 1152 of the section hard link through the Zechstein Group, while on the western side faults are
 1153 mechanically detached above and below the Zechstein Group salt. See figure 1 for seismic
 1154 line location. **Abbreviations:** IMS – Irish Mainland Shelf.



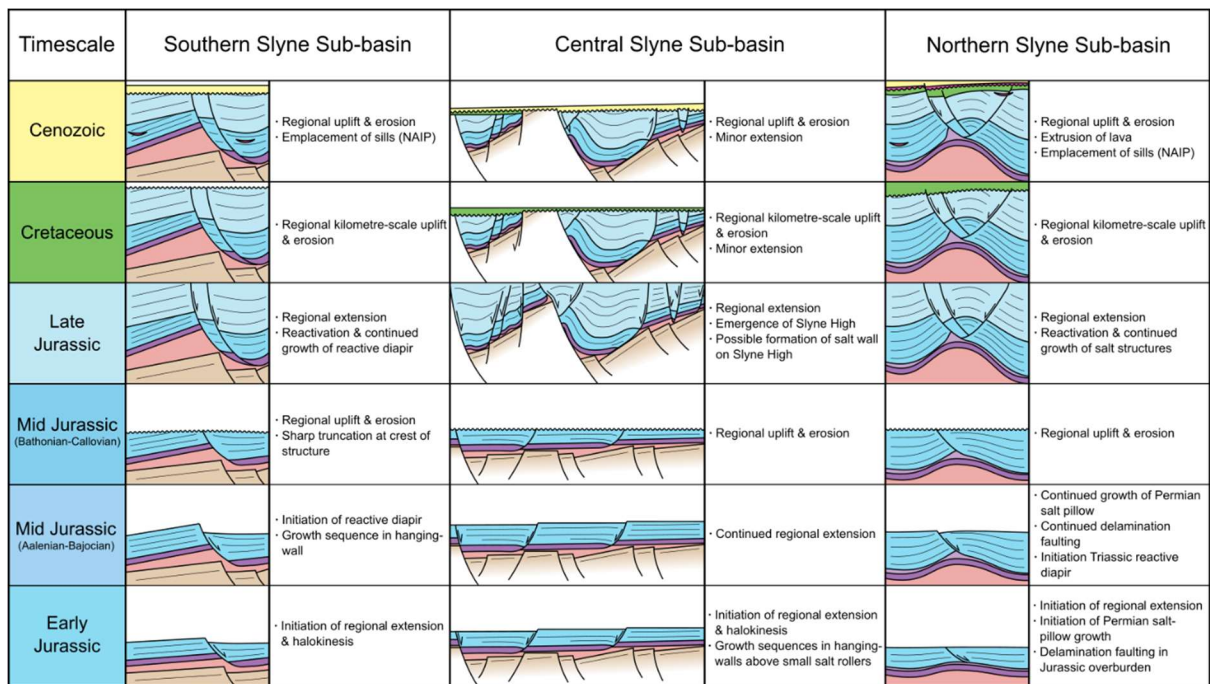
1155

1156 **Figure 11:** 2D seismic line PH98GPO133-027 and accompanying geoseismic section. The
 1157 northern Erris Basin dips westwards into the bounding fault along the margin of the Erris
 1158 Ridge, with a significantly reduced Mesozoic section preserved beneath the BCU. There is
 1159 little evidence of salt-related structures in this part of the basin. Eocene lavas cause significant
 1160 degradation of image quality. See figure 1 for seismic line location.



1161

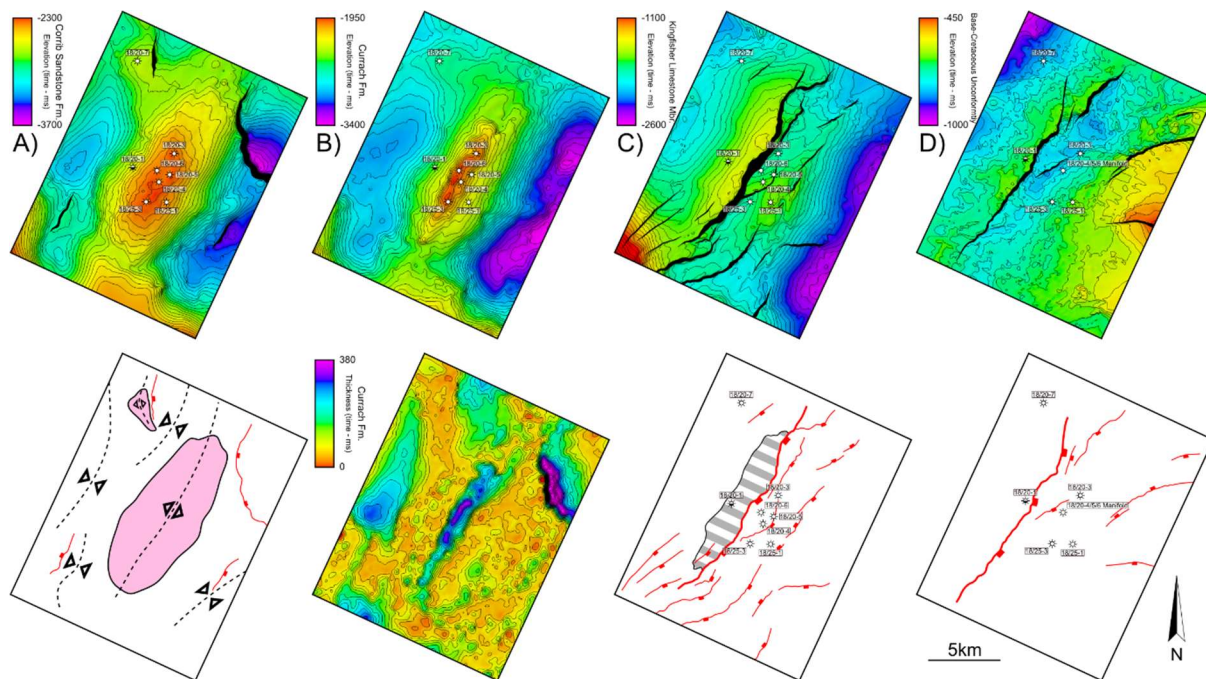
1162 **Figure 12:** 2D seismic line DBS99-304 and accompanying geoseismic section. Here the
 1163 northern Erris Basin is bounded by the Erris Ridge to the northwest and the Palaeozoic
 1164 Donegal Basin to the northeast, with a significantly reduced Mesozoic section preserved
 1165 beneath the BCU. There is little evidence of salt-related structures in this part of the basin.
 1166 See figure 1 for seismic line location. **Abbreviations:** ER – Erris Ridge.



1167

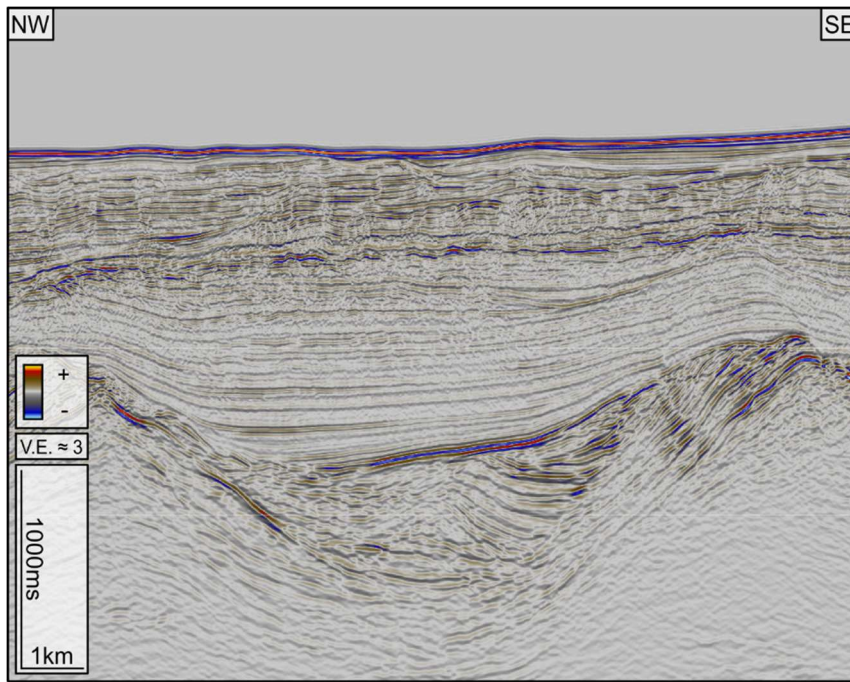
1168 **Figure 13:** Schematic evolutionary model for the formation of different salt-related structures
 1169 discussed in this study highlighting their multiphase structural evolution. Seismic lines through
 1170 the structures illustrated in the Southern, Central and Northern Slyne sub-basins are shown
 1171 in Fig. 6, 7A and 8B respectively

1172

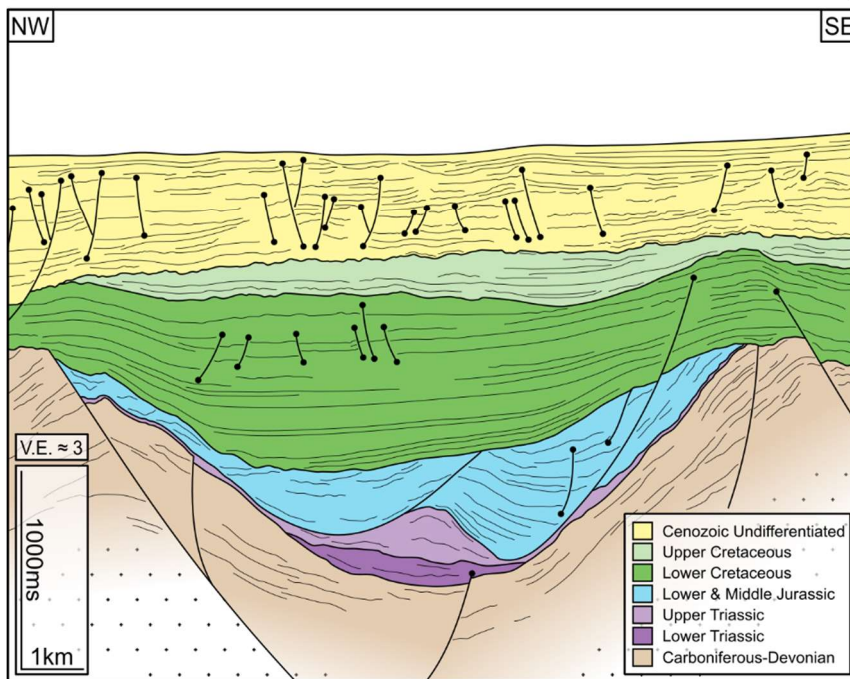


1173

1174 **Figure 14:** **A)** Time-structure map of the top Corrib Sandstone Formation and accompanying
 1175 map (below) showing the main Zechstein Group salt pillows. **B)** Time-structure map of the top
 1176 Currach Formation and accompanying TWTT thickness map (below) of the Currach
 1177 Formation. **C)** Time-structure map of the Kingfisher Limestone Member (near-base Upper
 1178 Jurassic) and accompanying fault map (below) with the structural closure in the hanging-wall
 1179 highlighted. **D)** Time-structure map of the Base-Cretaceous Unconformity and accompanying
 1180 fault map (below). Doming and faulting along the south-eastern edge of the survey is caused
 1181 by a shallow sill. See figure 1 inset for location.

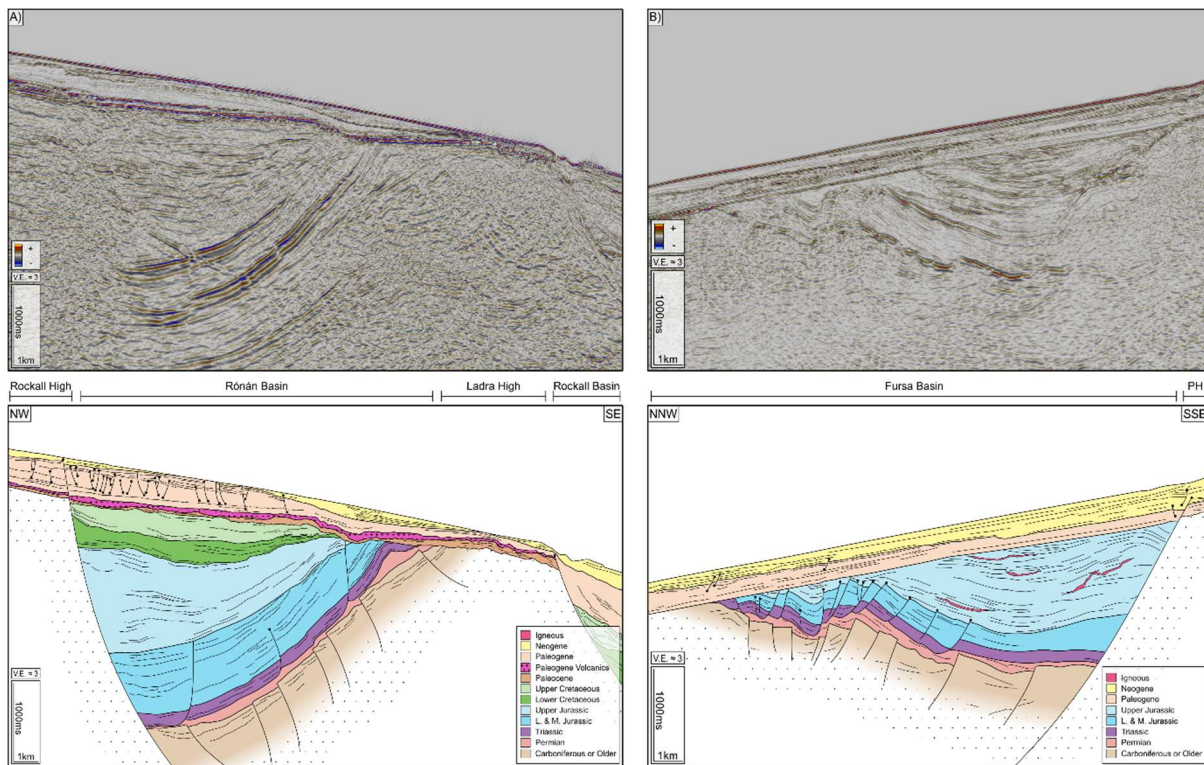


Goban Spur Basin



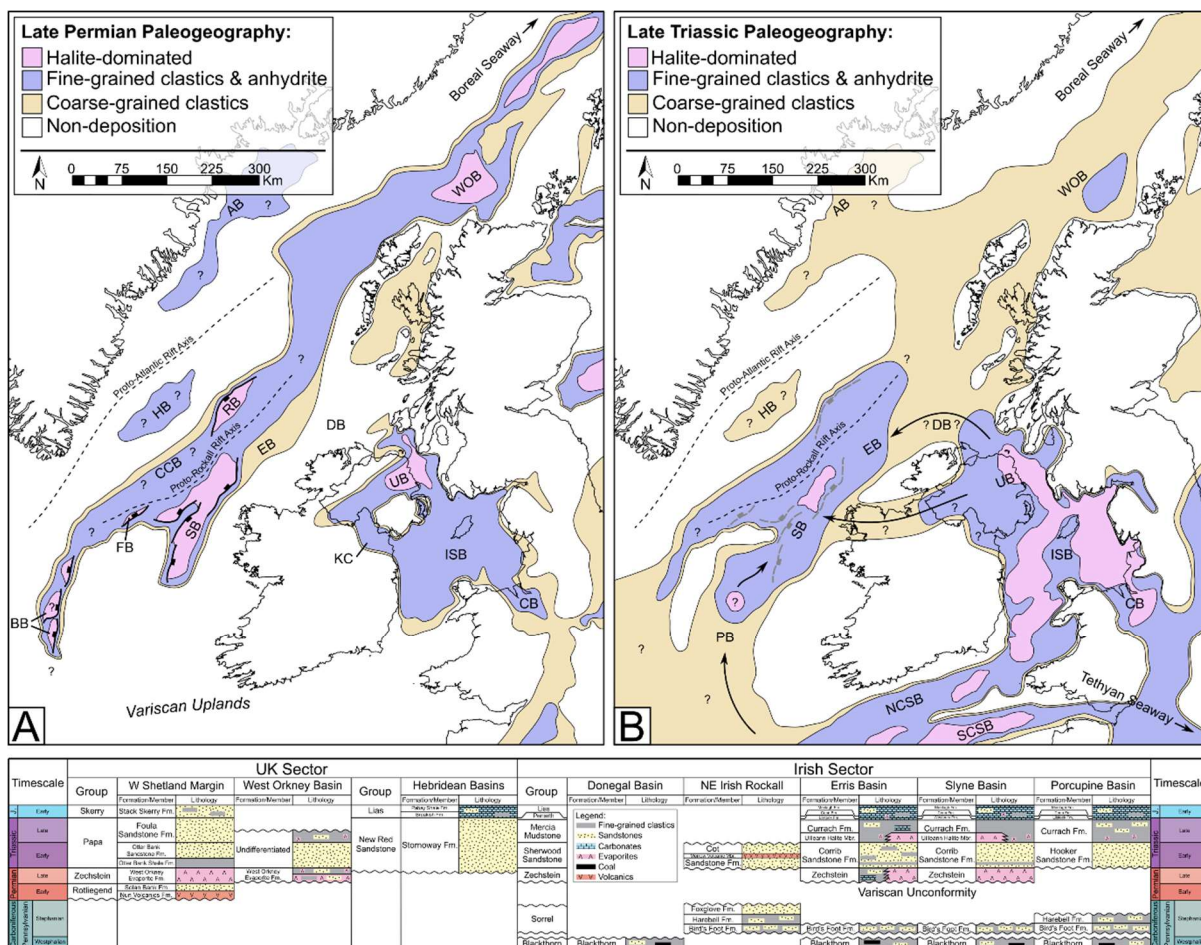
1182

1183 **Figure 15:** Part of 2D seismic line PAD13-044M and accompanying geoseismic section. A
 1184 distinct décollement surface is observed beneath the BCU. A salt pillow is also observed in
 1185 this section.



1186

1187 **Figure 16: A)** Part of 2D seismic line WRM96-107 and accompanying geoseismic section.
 1188 The Rónán Basin is located on the 'conjugate margin' of the Erris Basin on the north-western
 1189 margin of the Rockall Basin. **B)** Part of 2D seismic line IR11040 and accompanying
 1190 geoseismic section. A distinct décollement surface is interpreted in the Fursa Basin between
 1191 the bright top-basement reflector and the overlying Mesozoic section. **Abbreviations:** PH –
 1192 Porcupine High.



1193

1194 **Figure 17:** A) Schematic Late Permian paleogeographic map of the Irish Atlantic margin and
 1195 neighbouring regions showing the route of marine ingress from the Boreal Ocean to the Slyne
 1196 and Erris basins. B) Schematic Late Triassic paleogeographic map of the Irish Atlantic margin
 1197 and neighbouring regions showing three potential routes of marine ingress from the Tethys
 1198 Ocean to the Slyne and Erris basins. UK sector, Irish Sea and Celtic Sea basins adapted from
 1199 McKie, 2017. Greenland basins adapted from Gerlings et al., 2017. **Abbreviations:** AB –
 1200 Ammassalik Basin; BB – Bróna basins; CB – Cheshire Basin; EB – Erris Basin; FB – Fursa
 1201 Basin; HB – Hatton Basin; ISB – Irish Sea basins; KC – Kingscourt; NCSB – North Celtic Sea
 1202 Basin; RB – Rónán Basin; SB – Slyne Basin; SCSB – South Celtic Sea Basin; UB – Ulster
 1203 Basin; WOB – West Orkney Basin.